NASA Technical Memorandum 105156
AIAA-91-2456

Arcjet Thermal Characteristics

John M. Sankovic and Francis M. Curran
Lewis Research Center
Cleveland, Ohio

Prepared for the
27th Joint Propulsion Conference
cosponsored by the AIAA, SAE, ASME, and ASEE
Sacramento, California, June 24-27, 1991

NASA

ARCJET THERMAL CHARACTERISTICS

John M. Sankovic* and Francis M. Curran*
National Aeronautics and Space Administration
Lewis Research Center
Cleveland, Ohio 44135

ABSTRACT

The performance of radiation-cooled and water-cooled arcjet thrusters operating on both 1:2 nitrogen/hydrogen mixtures at 1-2 kW and on pure hydrogen at 1-4 kW were compared. For the radiation-cooled thruster, the thrust power recovered regeneratively was evaluated experimentally, and the anode losses were measured by the use of a radiant heat calorimeter. Anode power deposition was measured calorimetrically for the water-cooled design. The fraction of input electrical power lost to the anode increased with specific energy. In all cases, anode losses at a given specific energy level decreased with an increase in propellant flow rate. The data suggest that increases in flow rate decrease the anode losses by decreasing the anode fall voltage. The fraction of electrical power recovered regeneratively and converted to thrust decreased with increasing flow rate. To investigate the effects of test facility background pressure on performance, data were taken for both thrusters operating on nitrogen/hydrogen mixtures at facility background pressures nominally at 20 Pa and 0.20 Pa. Increasing the background pressure decreased the thruster performance, and simple pressure area corrections alone could not account for the observed degradation in performance. Increased facility pressures caused increased anode losses which may account for the remainder of the performance degradation.

INTRODUCTION

The arcjet thruster uses an electric arc to increase the enthalpy of the propellant. The hot gas is then expanded through a supersonic nozzle to convert the thermal energy in the gas to directed kinetic energy and thereby produce thrust.

During the late 1950's and through the mid 1960's, a great deal of research was conducted on arcjets in the range of 1-200 kW using a variety of propellants, including nitrogen, hydrogen, and ammonia. A comprehensive review of the early work in the field is given by Wallner and Czika[1]. The early work on arcjets was centered at 30 kW for primary propulsion missions. Because space power sources were not available to provide required power, work in arcjet thrusters was halted in the mid-1960's.

Because of the possibility of greater than factor of two increases in specific impulse without the need to redesign propellant storage and feed systems over other state-of-the art stationkeeping technology , 1 kW class hydrazine arcjet thruster research was rekindled in the mid-1980's. During this research effort a 1kW class hydrazine arcjet propulsion system, including a power processing unit (PPU), was developed[2]. The thruster exhibited a specific impulse of 450 s and had a lifetime greater than 1000 h over 500 cycles.[3]

Work is now underway to expand the mission applicability of the arcjet by expanding the power range and by investigating the possibility of using other propellants. High power arcjets operating on both hydrogen[4,5] and ammonia[6] are being evaluated for primary propulsion missions. Hydrogen is an attractive propellant because it offers much higher specific impulse values than storables; however, a great deal of work needs to be done in the area of cyrogenic propellant storage and thruster development. With advances in solar array technology, greater power may be soon available for electric propulsion, and research is being conducted to develop a 550 - 600 s hydrazine arcjet at 2 kW[7] and to investigate the performance of 1-5 kW hydrogen arcjets[8]. In anticipation of arcjet use on power limited satellites, a 300 W laboratory PPU has been developed,[9] and arcjets operating on 1:2 nitrogen/hydrogen mixtures have been shown[10] to reliably operate at power levels below 400 W.

In a typical arcjet only about a third of the input power is converted to thrust power. The remainder of the energy is lost to the electrodes, to frozen flow, and to nozzle inefficiency. One technique to increase the overall efficiency is to regeneratively recover the heat deposited into the electrodes. Using a water cooled low power arcjet simulator, Curran[11] investigated the electrode losses using nitrogen as the propellant. Electrode losses for high and low power hydrogen thrusters are reported in References 12 and 13. This study investigates the power deposition into the anode for a single arcjet geometry at power levels of 1-2 kW on 1:2 nitrogen/hydrogen

*Member AIAA

mixtures and 1-4 kW on pure hydrogen. The 1:2 nitrogen/hydrogen mixtures were used to simulate fully decomposed hydrazine. Using calorimetry, the power radiated off the anode housing of a radiation-cooled thruster was measured. The radiation-cooled thruster also provided information on the fraction of input power realized as thrust power due to regenerative effects. Using a water-cooled thruster, the anode power deposition was measured and the significant performance degradation, due to the cold nozzle walls, was noted. Finally, the effects of facility background pressure on performance for arcjets operating on 1:2 mixtures of nitrogen and hydrogen were investigated.

NOMENCLATURE

A	anode surface area, m^2
C_p	specific heat of coolant, J/kg-K
e	electron charge, C
F	thrust, mN
f_{cal}	percent of electrical power input into calorimeter
f_t	percent of electrical power realized as thrust power
f_r	percent of electrical power recovered regeneratively and converted to thrust
g	earth's gravitational acceleration, m/s^2
h_a	enthalpy of the gas layer near anode
h_{ps}	enthalpy of plasma stream
I	Arc current, A
I_{sp}	measured specific impulse, s
I_{spi}	ideal specific impulse, s
I_{spc}	cold flow specific impulse, s
k	Boltzmann constant, J/K
k_1	heat transfer constant, kg/m^2-s
m_p	mass flow rate of propellant, kg/s
m_w	mass flow rate of calorimeter fluid, kg/s
p	propellant inlet pressure, kPa
P_a	power loss to anode, W
p_b	facility background pressure, Pa
P_e	input electrical power, W
P_r	thrust power due to regeneration, W
P_{rad}	heat radiated to anode, W
Q_a	Power radiated off inside surface of nozzle, W
T_e	electron temperature, K
U_{af}	anode fall voltage, V
V	arc voltage, V
ΔT	difference between outlet and inlet temperatures, K
ϵ	emissivity
η_f	frozen flow efficiency
η_n	nozzle efficiency
η_o	total efficiency
η_t	thermal efficiency
Φ	work function, V

FUNDAMENTALS

As discussed by Wallner and Czika[1], the physics of the arcjet can be divided into three conceptual regions consisting of arc energy transfer, the thermodynamics of the propellants, and the aerodynamics of the flow. Figure 1 is a schematic of the energy deposition processes in the arcjet.

In an ideal thruster all input power would go into the fluid; however, because of electrode losses, this is not the case. The thermal efficiency can be defined as the ratio of the power into the fluid divided by the input power. It is important to note that the input power is the sum of the electrical power and the power of the inlet gas due to its enthalpy.

$$\eta_t = \frac{\text{Power in the gas}}{\text{Input power}} \qquad \text{(eq. 1)}$$

Due to frozen flow losses, only a fraction of the power in the gas can be used for thrust. This fraction can be defined as the frozen flow efficiency

$$\eta_f = \frac{\text{Power available for thrust}}{\text{Power in the gas}} \qquad \text{(eq. 2)}$$

Finally, the drag in the nozzle and divergence losses reduce the resultant thrust power to a fraction of the power available for thrust according to the nozzle efficiency

$$\eta_n = \frac{\text{Thrust power}}{\text{Power available for thrust}} \qquad \text{(eq. 3)}$$

The total efficiency can be defined as the ratio of thrust power to input power

$$\eta_o = \frac{\text{Thrust power}}{\text{Input power}}$$

$$= \eta_t \eta_f \eta_n$$

$$= \frac{Isp^2}{2P_e/g^2 m_p + Isp_i^2} \qquad \text{(eq. 4)}$$

Equation 4 reduces to the nozzle efficiency when the electrical power is zero. For the low

Reynolds number flows encountered in arcjets, this efficiency may be quite low and is expected to decrease as the gas temperature increases.

The energy lost to the cathode is typically quite small. Using a water-cooled cathode and nitrogen as the propellant, Curran[11] found that 1-5% of the input power was lost to the cathode. The loss was nearly constant with current, resulting in a decrease in the percent of power lost with increasing power level. The Dushman equation[14] describes thermionic emission as an exponential function of temperature. An increase in current is provided by a small change in cathode temperature, resulting in a slight increase in the total cathode power loss, but an overall decrease in the percentage.

The total heat input into the anode, neglecting ablation and Joule heating of the anode itself, is given by Shih[15] et al. as

$$P_a = P_{rad} + k_1 A(h_{ps}-h_a) + I\,[\,(5kT_e/2e) + \Phi + U_{af}] \quad \text{(eq. 5)}$$

The first term is net radiation the anode receives from the plasma and the cathode. The second term in the equation is due to convection between the gas and the nozzle wall, and the heat transfer is driven by the enthalpy difference between the anode surface and the gas. The direction and magnitude of heat transfer are dependent on location along the nozzle and the enthalpy of the incoming gas. A typical arcjet nozzle is of the de Laval type. In the converging section, the incoming gas is usually colder than the nozzle and the incoming gas enthalpy is increased regeneratively by heat transfer from the nozzle surface to the cold gas. In the diverging section, the bulk average gas temperature is much hotter than the nozzle wall so energy would probably be lost from the gas to the nozzle surface. Again, this is dependent on the temperature gradient in the boundary layer near the wall. The amount of heat recovered regeneratively is highly dependent on the propellant selected. For hydrogen, the heat capacity is large, and since it is stored cryogenically, the driving temperature difference available for regeneration will also be great. On the other hand, hydrazine has a lower heat capacity and its decomposition products leave the catalyst bed at a temperature of approximately 800 °C[16], making recovery of anode losses more difficult. The final term is the energy transferred by the electron current. It is composed of the energy the electrons possess due to their temperature at the edge of the anode fall region, the energy gained through the anode fall, and energy gained by the electrons entering the surface of the anode.

For a radiation-cooled arcjet, assuming the anode is thermally insulated and the thruster is at steady-state operating conditions in a hard vacuum, the energy radiated off the anode surface is the net energy lost to the anode given by eq. 5. Using a calorimeter which absorbs all of the energy radiated off anode surface, the energy lost to the anode can be expressed as

$$P_a = C_p\, m_w\, \Delta T \quad \text{(eq. 6)}$$

A water-cooled thruster is by design a calorimeter, and by knowing the coolant mass flow rate and the inlet and outlet temperatures, the energy deposition to the anode can be determined from eq. 6. The energy input into a water-cooled thruster anode is always much greater than the energy lost to the anode in a radiation-cooled design. With a water cooled design the convective term in eq. 6 becomes dominant. No heat is returned to the propellant regeneratively and a greater amount is removed in the diverging section, since the driving temperature difference is larger with a cold nozzle wall.

In optimizing the design of an arcjet, knowledge of amount and location of input energy deposition is crucial. The results reported herein are presented as fractions of the input electrical power. The thrust power data reported are the thrust due to the input electrical power. To accomplish this the kinetic energy component due to the enthalpy of the inlet gas is subtracted from the thrust power; therefore, the fraction of input electrical power realized as thrust is given by

$$f_t = \frac{I_{sp}^2 - I_{spc}^2}{2P_e/\,g^2\, m_p} \quad \text{(eq. 7)}$$

The amount of regeneration for a radiation-cooled thruster is highly dependent on the design of the thruster, specifically upon the path the propellant takes prior to injection. These regenerative effects can be approximated experimentally by measuring the thrust power after arc extinction[17]. The thrust power measured immediately after the arc has been extinguished is much greater than the cold gas thrust power because the gas picks up heat regeneratively from the hot thruster components as it enters, increasing its enthalpy before expansion. The fraction of input electrical power recovered

regeneratively and converted to thrust is given by eq. 7 when the Isp is the corresponding specific impulse immediately after the arc is turned off and the flow stabilizes.

EXPERIMENTAL APPARATUS

Arcjet Thrusters. The arcjet thrusters used for this study were of the same constricted-arc, vortex stabilized, modular design which have demonstrated lifetimes of over 1000 h on simulated hydrazine mixtures[3]. A schematic appears in Figure 2. The anode,which served as the nozzle, was fabricated from a solid piece of 2% thoriated tungsten. It consisted of a conical converging section with a 30° half angle, a contrictor section, and a conical diverging section with a half angle of 20°. Initially the nozzle had a throat diameter of 0.064 cm, a constrictor length of 0.025 cm, and an area ratio of 225.

The cathode was a 0.318 cm diameter, 2% thoriated tungsten rod with one end tapered to a 30° half angle. Insulation between the cathode and the anode was accomplished using high grade pure boron nitride in the front of the thruster where the temperatures were the greatest and boron nitride fixed with a calcium binder in the rear of the thruster. The arc gap[18] was set using a modified fluid fitting with a ferrule at the rear of the thruster.

The radiation cooled arcjet used an anode housing fabricated from arc cast titaniated, zirconiated molybdenum (TZM). For the water cooled arcjet, the anode housing material was copper. Eight turns of 0.635 cm O.D., 0.472 cm I.D. tubing were soft soldered to the copper housing to provide cooling, and to form a calorimeter to measure the anode heat losses. Figure 3 is a photograph of the water-cooled thruster.

Radiant Heat Calorimeter. The calorimeter used to measure the radiant heat loss from the anode housing is shown in Figure 4. It consisted of a copper enclosure which slid over the anode housing and bolted to the arcjet. Copper tubing of 0.635 cm O.D. was soft soldered to the enclosure to provide passages for cooling. The front of the calorimeter had an opening 1.3 cm in diameter. The front and rear openings of the calorimeter were slightly larger than the nozzle and anode housing outer diameters, respectively, to prevent contact. The only conduction path which existed was through the stainless steel threaded rod used to hold the calorimeter to the thruster and the thruster together. It is assumed that conduction losses are negligible due to the low temperature at the rear of the anode housing and the poor thermal conductivity of stainless steel. The inside surface was coated with graphite in the form of an aerosol spray to increase the emissivity.

Arcjet Power Processor. The design for the power processing unit used for this study is described by Gruber[19]. It used a pulse-width modulated power converter which was closed-loop configured for fast current control. The maximum output current was 50 A and the open circuit voltage was 180 V. Arc ignition was accomplished using a high voltage pulse, nominally 3.5 kV.

Thrust Stand. A displacement type thrust stand of the type desribed by Haag and Curran[18] was used to obtain the thrust measurements. The arcjet was supported by an up-right flexure arrangement and displacement was measured using a linear variable differential transformer over an active range of approximately 5 mm.

Vacuum Facility. The tests were conducted in a 1.5 m diameter by 5 m long cylindrical vacuum vessel, equipped with four 0.82 m diameter oil diffusion pumps each with a pumping capacity of approximately 32 m^3/s at 0.19 Pa. The diffusion pumps were backed by a 0.61 m^3/s at 1.3 Pa rotary blower and two 0.14 m^3/s capacity roughing pumps.

Instrumentation and Calibration. The arcjet voltage was measured to an accuracy of 0.1 V at the inlet to vacuum facility using a digital multimeter. Arcjet current was measured using a Hall effect current sensor which was calibrated before each run using a current shunt, and the reported values are accurate to 0.1 A. Propellant flow regulation was accomplished using commercially available thermal conductivity type mass flow controllers (5 SLPM full scale) for the 1:2 nitrogen/hydrogen tests and a needle valve in series with a thermal conductivity type flow meter (50 SLPM full scale) for the pure hygrogen tests. Calibration of the mass flow measurements was done in-situ several times during the test series using a constant volume tank. The flow measurement was accurate to 1%. The thrust was calibrated using three dead weights each with a mass of 4.0 g. Thrust measurements were accurate to 1%. The arcjet propellant inlet pressure was measured at the inlet to the vacuum facility using a 0-1400 kPa full scale pressure transducer. Tank pressure was measured with a capacitance manometer with a 0-133 Pa range. Two ionization gauges were also

used to monitor tank pressure and gave values that were approximately a factor of two lower than the capacitance manometer. The capacitance manometer values should be gas independent, while the ionization gauges need to be calibrated to a specific gas which is difficult for mixtures. All pressure values reported herein were obtained using the capacitance manometer.

Water was used as the cooling fluid for both calorimeters, entering the at the front of the thruster and exiting at the rear of the anode housing. Circulation and inlet temperature regulation were accomplished using a commerically available water circulator with temperature regulation and a rated heat capacity of 520 W. The inlet water temperature to both calorimeters was nominally 19°C. Water flow was measured with a turbine type flow meter which was calibrated on water in-situ by flowing the water into a container over a given time interval and weighing the container. Calibration was done over the full range of flow rates and spot checked throughout the test sequence. The flow measurement was accurate to ±5%. The inlet and outlet temperature of the water was measured using ungrounded chromel-alumel thermocouple probes. The probes were mounted using a tee fluid fitting. The probes were inserted over 1.5 cm past the elbow into the water before the bend in the tee in to insure proper measurement of the average water temperature. Care was also taken to prevent air pockets in the vicinity of the temperature probes. The outputs of the thermocouples were connected to a two position switch and then to a commercially available temperature readout, sensitive to 0.06 °C.

EXPERIMENTAL PROCEDURE

Initially the radiant heat calorimeter was not insulated from the ambient gas in the vacuum chamber. Tests conducted at background pressures nominally ranging from 0.20 Pa to 20 Pa showed large increases in the power input to the calorimeter as the pressure varied. The problem was due to convection from the hot exhaust gas to the cold copper surface of the calorimeter. At the higher background pressure, the convection caused the heat input to the calorimeter to be two to three times higher than at the lower background pressures. When alumina fiber blanket insulation was applied to the calorimeters the data converged. The insulation was attached using a combination of quartz ceramic adhesive and silicon tape. A typical insulation thickness was between 0.16 cm and 0.32 cm. All data reported were obtained using the insulated calorimeters.

The first test series was done with the radiant heat calorimeter. The arcjet used had been run on both 1:2 nitrogen/hydrogen mixtures and on hydrogen for over 20 h prior to taking any data. Data were taken at hydrogen propellant flow rates of 22.5, 15.0, and 10.0 x 10^{-6} kg/s. These flow rates exceeded the pumping capacity of the diffusion pumps and the pumps were not used. The tank pressure was 45, 31, and 20 Pa for the three mass flow rates, respectively. The effects of background pressure were investigated by taking data with the diffusion pumps on and off using nitrogen/hydrogen mixtures as the propellant. Data were taken at flow rates of 61.7, 49.0, and 36.4 x 10^{-6} kg/s with the diffusion pumps off, resulting in respective pressures of 25, 20 and 16 Pa. The 61.7 x 10^{-6} kg/s flow rate was too great for the diffusion pumps; consequently data were taken only at 49.0 and 36.4 x 10^{-6} kg/s at the low background pressures of nominally 0.23 and 0.15 Pa. Data were typically taken at the highest power and greatest flow rate first, then in order of decreasing power level at each flow rate. At the end of a test series a datum point was commonly repeated to check the reproducibility of the data. The data from the repeated points are also included herein. The thruster and the calorimeter temperatures came to steady state within ten minutes of a change in operating condition.

Immediately after extinguishing the arc the thrust reading was greater than the cold flow value, due to regenerative heating of the incoming gas by the hot thruster walls. To measure the resultant thrust due to regeneratively recovered energy, the thrust was recorded on a strip chart recorder and the difference between the thrust with the arc on and 2 s after the arc had been extinguished was noted. The 2 s time lapse was needed for the active damping in the thrust stand and the flow to stabilize. Each datum point therefore required a restart of the thruster. The thrust zero was also noted before and after each operating condition to account for any thermal drift in the thrust measurement. The uncertainty in the measurement was about ±1.2 mN due to the resolution on the strip chart recorder.

Performance data were not taken with the calorimeter mounted on the arcjet. The increased weight, the tubing for the water lines, and the thermocouple leads would have caused additional error in the thrust measurement. After all data were taken for the radiant heat calorimeter, it was

removed, and the thruster performance was determined. Basically, the same test sequence was followed for the performance tests as for the calorimeter tests. Hydrogen data were taken first, then high background pressure nitrogen/hydrogen mixture data, and finally the low background pressure mixtures.

After the performance tests of the radiation cooled arcjet were accomplished the thruster was disassembled and the electrodes inspected. The nozzle diameter had eroded to 0.077 cm and the arc gap had increased to 0.098 cm. The overall length of the thruster was not recorded, and it is uncertain if the entire increase in arc gap was due to cathode erosion or partly due to the nozzle insert being pushed farther into the housing during thermal cycling. Degradation of the front graphite foil seal was also noted; however, a leak check of the thruster at the end of testing showed no reduction in the fidelity of the joint. No noticable chemical interaction occured between the cathode and the boron nitride insulator.

The arcjet was then reassembled using the water-cooled copper anode housing. The same electrodes were used; however, the graphite foil seals were replaced. The arc gap was reset at the 0.077 cm, the mean gap of the previous test matrix. The same insulating procedure used for the radiation calorimeter was also used to prevent convection from the exhaust to the anode calorimeter.

Performance measurements were taken concurrently with anode power deposition data. The water cooling lines were flexable polymer tubing and were hung down from the top of the vacuum vessel along with the thermocouple lines. Heating of the polymer tubing caused zero drifts in the thrust. To account for these changes, the thrust zero was checked before and after each data point was taken, requiring restarting the thruster after each operating point. The same basic test matrix used in the radiant heat calorimetry tests was also used for this test series. Pure hydrogen data were taken at propellant flow rates of 22.5 and 15.0 x 10^{-6} kg/s. The lowest flow rate of 10.0 x 10^{-6} kg/s was tried,at current levels below 25 A, but steady operation could not be achieved due to the lower chamber pressure in the water cooled thruster compared to the radiant heat thruster. Data were taken with 1:2 nitrogen/hydrogen as the propellant at flow rates of 61.7 and 49.0 x 10^{-6} kg/s at background pressures on the order of 20 Pa , and at a flow rate of 49.0 x 10^{-6} kg/s at a nominal background pressure of 0.20 Pa. Again the lowest flow rate of 36.4 x 10^{-6} kg/s was eliminated because the chamber pressure was too low for arc stability given this thruster geometry, and the 61.7 x 10^{-6} kg/s flow rate was above the pumping capacity of the diffusion pumps. The water cooled thruster stabilized very quickly and data were taken at ten minute intervals. Post-test disassembly of the water-cooled thruster showed no increase in arc gap.

RESULTS AND DISCUSSION

Hydrogen Propellant. The performance data for the radiation and water-cooled thrusters are provided in Tables I and II, repectively. The cold gas performance is given in Table III and was found to be the same for both thrusters. All values reported for performance are measured values, and no correction was made to account for the facility background pressure. The effects of facility background pressure on the performance of hydrogen arcjets is discussed in Reference 8. The thrust values reported in the two tables are the total thrust values, not the thrust due solely to the input electrical power. Specific impulse as a function of input specific energy to the propellant for both the water-cooled and radiation-cooled arcjets is plotted in Figure 5. The performance data of the radiation-cooled thruster compares well with data reported by Curran[8] et al. The plots show that performance at a given specific energy decreases with flow rate for both thrusters. A slight decrease in specific impulse is noted between 22.5 and 15.0 x 10^{-6} kg/s but a much larger difference exists between 15.0 and 10.0 x 10^{-6} kg/s. The water cooled thruster data follows the same trend as the radiatively cooled thruster data; however, the data are shifted by a nearly constant amount. At a specific energy of 150 MJ/kg the difference between the hot walled and cold walled thruster specific impulse is 196 s at 15 x 10^{-6} kg/s and 194 s at 22.5 x 10^{-6} kg/s.

A plot of the voltage-current characteristics of the two thrusters is given in Figure 6. Due to the increased pressure, at a given current, the voltage increases with flow rate. At a given current and flow rate, the voltage is over ten volts lower for the water-cooled thruster than for the radiation-cooled thruster. Again this difference in voltage can be attributed to the difference in chamber pressure. Referring to the inlet pressure data in Tables I, II, and III the inlet pressure is 40-70 kPa greater than the cold flow value for the water-cooled thruster while the pressure increase with the arc on is 100-200 kPa for the radiation-cooled design. Although these pressure data are

not the values in the arc chamber, the trends represented are directly applicable.

Figure 7 shows the percent of input electrical power realized as thrust versus specific energy. Since the thrust power at a given specific energy is a function of the specific impulse, the trends shown in Figure 7 are similar to those shown in Figure 5. For the radiation cooled thruster at an input specific energy level of 150 MJ/kg, and at flow rates of 22.5, 15.0, and 10.0 x 10^{-6} kg/s, the percent of input electrical power which is converted to thrust is 30.5%, 27.6%, and 22.1%, respectively. For the water-cooled arcjet, 19.2% and 16.7% of the input electrical power was converted into thrust at the same specific energy level and flow rates of 22.5 and 15.0 x 10^{-6} kg/s. Thus, the water-cooled thruster was found to convert less than two-thirds as much of the input electrical power into thrust power as its radiation cooled counterpart. In the hot walled thruster some of the energy input into the anode regeneratively heats the incoming gas. This is evidenced by increased inlet pressure. None of the anode input power for the cold walled thruster is recovered regeneratively since the incoming gas temperature is approximately equal to the wall temperature. Instead, heat is lost from the hot gas since the temperature gradient between the gas and the nozzle wall is greater for the water-cooled thruster than for the radiation-cooled design.

By measuring the thrust of the radiation-cooled arcjet soon after the arc is extinguished, the amount of anode input power converted regeneratively to thrust was determined. The data are given in Table I. Figure 8 shows the amount of thrust recovered regeneratively as a percent of the input electrical power for all three propellant flow rates as a function of input specific energy. Intuitively, it would be expected that a greater fraction of energy would be recovered at the higher mass flow rate, due to convective effects. Even if the fractional amount of energy recovered by the gas from the hot anode was the same for all flow rates, the realized thrust should be greatest for the highest flow rate due to the decrease in viscous effects and increase in nozzle efficiency. The cold flow data shows that as the flow rate increases the specific impulse also increases, due to a decrease in viscous losses. The opposite trend, however, is shown in Figure 8. As the propellant flow rate increases the fraction of input power recovered regeneratively and converted to thrust decreases. A likely explanation for these results is that at the same input specific energy fractionally less energy is being deposited into the anode as the flow rate increases.

Calorimetric data for both the water-cooled thruster and for the radiation-cooled thruster substantiate this explanation. The data obtained using the radiant heat calorimeter and the radiation-cooled arcjet are presented in Table IV, while anode power deposition data for the water-cooled thruster are given in Table V. Figure 9 shows the fraction of input electrical power deposited into the water-cooled anode as a function of the input specific energy for propellant flow rates of 22.5 and 15.0 x 10^{-6} kg/s. Clearly, a smaller percentage of the input power is lost to the anode for the 22.5 mg/s flow rate than for the 15.0 x 10^{-6} kg/s flow rate. Figure 10 shows the data obtained using the radiant heat calorimeter with the radiation-cooled arcjet. The fraction of input power radiated from the anode housing decreases as the flow rate increases. Both Figures 9 and 10 show that as the specific energy increases, the percent of input power lost to the anode also increases. This is true for all flow rates; however, the rate of increase is lowest for the highest flow rate.

As mentioned previously, the specific impulse versus specific energy curves for different propellant flow rates begin to diverge as the specific energy increases. This phenomenon has been documented in other studies of arcjet performance[7,10]. Figure 5 shows that at given specific energy, the highest specific impulse, and consequently the highest efficiency, always occurs at the highest flow rate. Different slopes of the curves in Figure 10 could provide an explaination for the divergence of the specific impulse versus specific energy performance curves.

It is clear that the amount of energy lost to the anode is highly dependent on flow rate; however, the reason for this has not yet been addressed. An attempt was made to determine which of the three terms in eq. 5 is dominant in energy transfer to the anode. Operation at a current level of 30 A and a flow rate of 22.5 x 10^{-6} kg/s was chosen as the test point, and the resultant total power was 3430 W from Table I. The power input to the anode is the sum of the heat radiated off the surface, the heat conducted through the power leads, and the heat recovered regeneratively into the gas. From Table IV, the power radiated off the thruster and captured by the calorimeter at 30 A was 210 W. To account for conducted losses and radiated power not sensed by the calorimeter a factor of 3% of the input electrical

power was used which amounted to 103 W. Jusification for the 3% factor is provided in the section entitled Closure and Uncertainties. From Table I, the power recovered regeneratively and converted to thrust was 205 W. Dividing this by an estimate of the nozzle efficiency gives the power recovered regeneratively from the anode. Using a nozzle efficiency of 0.7, gives a value of 293 W for the regenerative power. The total power input into the anode at this operating condition was 606 W.

From eq. 5, the power deposited into the anode by the current carrying electron is the sum of the power due to the thermal energy of the electrons, the work function, and the anode fall. Data for the electron temperature inside a low power hydrogen arcjet are not available; however, Zube and Myers[20] using spectroscopic techniques found that the electron temperature inside a low power arcjet of the same nozzle geometry operating on nitrogen/hydrogen mixture was between 1 and 2 eV. Using a value of 1.5 eV, the contribution of this term to the anode power loss was calculated to be 113 W. For 2% thoriated tungsten the work function is estimated to be 3.3 V[21], and at 30A this results in an anode loss of 99 W. Curran and Manzella[22] using a segmented low power arcjet operating on nitrogen/hydrogen mixtures approximated an anode fall voltage of 10-15 V. Since no data are available on hydrogen, a mean value of 12.5 V was assumed which implies a loss component of 375 W. The total anode loss due to the current carrying electrons is 587 W. Comparing this number to the total anode power loss determined in the previous paragraph, it is clear that relatively little power is deposited into the anode from radiation and convection. When considering the net anode losses, the convective term is negative as a result of regenerative heating in the converging section of the nozzle.

This simplified analysis of the anode losses given by eq. 5 shows that the convective and radiative terms are not dominant, the question now presented is which of the three components in the third term are affected by a change in propellant flow rate. No data are available inside the nozzle for the effect of flow rate on electron temperature; however, using electrostatic probes in the near field plume of a low power arcjet operating on nitrogen/hydrogen mixtures, Sankovic[23] found that the electron temperature did not vary significantly with flow rate. The work function is not a function of flow rate directly, but it is a weak function of surface temperature. At a given specific energy level the temperature of the anode surface may change with propellant flow rate. To the first order, the effect of flow rate on work function losses is negligible. The only remaining component of the electron current loss term is the anode fall. The anode fall is believed to be affected by the flow rate. Work with segmented anode arcjets[22,24] has shown that as the mass flow rate is increased the arc attachment point is forced farther downstream, which appears to result in a decrease of the anode fall.

Nitrogen/Hydrogen Mixture Propellant. Data were taken for both the radiation-cooled and water-cooled thrusters at two different facility background pressures, and the effects of facility pressure on performance will be addressed in this section. Tables VI and VII provide the performance data for the radiation-cooled thruster at high and low facility pressures, repectively. The same data are given in Tables VIII and IX for the water-cooled arcjet. The cold gas performance data are given in Table X. The specific impulse as a function of input specific energy for both the water-cooled and radiation-cooled thrusters operating at pressures in the 20 Pa range is provided in Figure 11. The same data for low facility background pressure operation at approximately 0.20 Pa are plotted in Figure 12. Both figures show the same trends as the hydrogen data. At all propellant flow rates tested, the specific impulse is approximately 100 s greater for the radiation-cooled thruster. Also, for both thrusters, at a given specific energy, the Isp asymptotically increases with flow rate.

The voltage-current characteristics for the radiation-cooled thruster operating at various flow rates at both low and high facility background pressures are given in Figure 13. As expected, at a given current level the voltage increases with increasing flow rate, due to an increase in impedance and an increase in arc length. At a given current and propellant flow rate, the voltage seems slightly higher at the low background pressure. This is probably not due to a facility effect, but is probably due to a change in arc gap with time. The low background pressure data were taken after the high background pressure test series, and the voltage is higher, simply due to changes in the electrode gap. Evidence of this is presented in the data taken at 49.0 x 10^{-6} kg/s, low background pressure data. Data were taken at all points in the test matrix, and at the end of the series the 10 A point was repeated and an increase in voltage of 1.0 V was noted.

The difference in V-I characteristics for the water-cooled thruster and the radiation-cooled arcjet are shown in Figure 14. For a given flow rate and current, the voltage is significantly lower for the water-cooled thruster, and the difference increases with an increase in current. An explaination for this is the dependence of arc voltage on chamber pressure. A small increase in current for the radiation-cooled arcjet causes a much greater increase in pressure when compared to the water-cooled design. At high flow rates and low power levels, the thruster runs much cooler and the pressure difference is much smaller, and this explains the convergence of the V-I characteristics. This phenomenon was not noticed in the pure hydrogen data. Since regenerative effects were larger in a hydrogen thrusters, even at low current and high flow rates, the chamber pressure was always much greater in the radiation-cooled thruster than the water-cooled design.

A measure of the overall efficiency is given by the plot of the percent of input electrical power coverted to thrust versus specific energy shown in Figure 15 for the high facility background pressure and in Figure 16 for the low facility pressures. As in the case of hydrogen, it is clear that for the radiation cooled design the electrical power realized as thrust power increases asymptotically with flow rate. Again, this is likely due to lower anode losses at higher flow rates. This will be shown by data discussed later in this section. Not enough data are available to determine a trend in propellant flow rate for the water-cooled thruster. However, a comparison can be made between the performance of the two arcjets. At an operating point of 30 MJ/kg and a flow rate of 49.0 mg/s, 32.6% of the input electrical power was converted to thrust in the radiation-cooled arcjet, while only 26.4% was realized as thrust power for the water-cooled design. Due to increased heat transfer from the gas to the nozzle, at a given flow rate over 6%, approximately one-fifth, of the absolute input electrical power is realized as thrust for the radiation-cooled thruster. This is very significant for a thruster with a nominal efficiency in the thirty percent range. Comparing operating performance at high and low facility pressures, it can be seen that the percent of input power converted to thrust is approximately two absolute percentage points higher at the low background pressure for both thrusters and all flow rates.

The difference in performance due to facility background pressure is greater than can be explained by a simple pressure area correction, assuming the exit pressure to be the ambient facility pressure. For example, assuming the pressure at the nozzle exit plane is the facility pressure of 1.5 Pa and all the pressure energy is converted to directed kinetic energy, the increase in efficiency would be slightly over 1%. Because of nozzle losses the amount would actually be much less. Clearly this does not account for the over 2% difference in efficiency between the data shown in Figures 15 and 16. The additional energy is thought to be lost to the anode due to increased heat transfer at high facility background pressure, and data to substantiate this are presented in the following paragraphs.

The energy deposition into the water-cooled thruster anode for high and low background pressures are presented in Figure 17. The calorimetry data are provided in Tables XI and XII. For the 49.0 x 10^{-6} kg/s flow rate a very definite increase in anode power deposition with an increase in specific energy is noted. An abnormality in the data at 61.7 x 10^{-6} kg/s is noted. It is believed that is a real effect and not simply scatter in the data. The corresponding decrease in anode power deposition at specific power levels greater than 25 MJ/kg noted in Figure 17 is also shown as a decrease in in performance in Figure 16. The fact that the data taken at 25 MJ/kg is repeatable and the same discontinuity is demonstrated using two independent testing methods leads to the conclusion that it is a real effect. Whether the discontinuity signals a change in the physics and can be repeated is yet to be determined. It does appear that approximately one percent more power is deposited into the anode at the higher background pressure.

Finally, the percent of input electrical power radiated off the anode housing as a function of specific energy is given in Figure 18. Again it is clear that as the flow rate increases at a given specific energy level, the power lost to the anode decreases for the range of flow rates tested as is shown by the data in Tables XIII and XIV. Also, there is a significant difference between the amount of energy lost to the anode of an arcjet operating at low and at high background pressures. Over two percent more of the total input energy is lost to the anode when the background pressure is high.

The performance data for both thrusters show a definite degradation in efficiency by increasing

the facility background pressure which cannot be completely explained by a pressure correction. Data from the radiant heat calorimeter and from the water-cooled thruster indicate an increase in anode losses. These increased losses are most probably due to the convective term in eq. 5. It can be assumed that since the arc voltage is not affected by the facility pressures tested, the anode loss components due to the current carrying electrons and to radiation do not change significantly. For a radiation-cooled thruster, the temperature of thruster decreases as the facility pressure increases. This is due to convective cooling of the outside of the thruster which results at high background pressures. The colder anode wall results in increased heat transfer from the hot gas and decreased regenerative heating, increasing net anode losses. The energy transfer in a resistojet is analogous to the regenerative heating in an arcjet. Manzella[25] et al. found that as the ambient pressure increased, the internal temperatures, and thus the thermal efficiency, in the resistojet decreased due to convective cooling of the outside surface by the ambient gas.

Because the anode is held at basically a constant temperature in the water-cooled thruster, this effect should not be seen in those data. However, Figure 17 shows about a 1% difference in percent of anode losses for the cold walled-thruster. It is quite possible that some of the additional heat transfer detected in the calorimeters at higher pressures was due to heat transfer from the hot exhaust gas to the copper surface, even though it was insulated. This would explain the 1% difference in the water-cooled data, but does not change the conclusions of the radiation-cooled data, since the difference was over 2% for that thruster. To fully quantify the phenomenon, higher sensitivity tests need to be performed over a wider range of facility background pressures.

Figure 19 shows the percent of input power recovered regeneratively and converted to thrust for the radiation-cooled thruster operating at high at low background pressures. No attempt is made to suggest any effect of facility pressure on regeneration, since more data with lower uncertainty are needed. Similar to the hydrogen data, the percentage of power regeneratively converted to thrust increases significantly with a decrease in flow rate for both thrusters. Again this is believed to be due to a decrease in power deposited to the anode with an increase in flow rate. It should be stressed that these data are for a nitrogen/hydrogen mixture entering the thruster at room temperature. In a flight-type arcjet the temperature of the decomposed hydrazine will be several hundred degrees Celsius, and the regenerative gains will be small and highly dependent on the design. Therefore, the absolute values reported herein are unimportant, but the trends should be directly transferable from the laboratory to the flight design.

Closure and Uncertainties.

The accuracies of the equipment used and the calibration techniques have been reported in previous sections. The need for insulation on the calorimeters due to the adverse effects of covective heat transfer from the hot exhaust gas to the calorimeters has also been noted. This section addresses losses which were not measured, but may be important. Also, using performance and calorimetric data for both the water-cooled and radiation-cooled thrusters, closure of the data is demonstrated through energy balances.

The net anode power deposition for the nitrogen/hydrogen mixture operation were a great deal lower than for hydrogen since the input electrical power was a factor of two lower. Hence the calorimetry data for the mixtures has a greater uncertainty due to the smaller temperature gradients in the coolant.

The radiation calorimeter neglects energy conducted back through the rear insulator and copper power cables and the power radiated from the inside of the nozzle to space. Also as is seen in Figure 4 a small section of the TZM anode housing was exposed. The exposed anode housing had a surface area of about 0.0028 m^2. The emissivity at the assumed surface temperature was linearly interpolated from the values provided in Ref. 26. For most of the operating points this surface did not glow and a temperature of 900 K was assumed, giving an emissivity of 0.11. This results in a power loss of 12 W which was not captured by the calorimeter. For some of the low flow rates at high power levels, the temperature may have reached 1200 K and corresponding emissivity would have reached 0.14, giving a power loss of 46 W.

The heat conducted back into the rear insulator and radiated off the boron nitride surface was small. Given an approximate surface area of 0.0076 m^2, an emissivity of 0.1 and a temperature of 700 K, the resulting power loss was calculated to be 12 W.

To compute the heat conducted through the power cables, the length was assumed to be 0.61 m with a cross-sectional surface area of 0.32 cm^2 an end temperature of 50 °C, and a thermal conductivity of 370 W/m-°C. The anode lead was assume to have an end temperature of 600 °C, and the cathode lead was assumed to be 200 °C at the connector. This gives a conductive heat loss of 11 W for the anode lead and 3 W for the cathode lead.

Finally an attempt was made to estimate the power radiated from the inside surface of the nozzle. The view factor assuming constant surface temperature for the lateral frustum surface to space was obtained from Bien[27]. The emissivity of the surface as a function of temperature was extrapolated from data provided in Ref. 26. Using the Stephan-Boltzmann law[26], the results for surface temperatures ranging from 1000-3000 K are provided in Table XV. An assumption of 2000 K for the nozzle temperature is reasonable for most of the operating points of radiation-cooled thruster, and this results in 19 W being radiated off the inside surface to space and not captured by the calorimeter.

Closure of the data was checked for hydrogen operation at a specific energy level of 150 MJ/kg and a propellant flow rate of 22.5 x 10^{-6} kg/s. Since data points at that exact operating condition were not available, linear interpolation was used. For the water-cooled thruster 19.2% of the electrical power was converted to thrust, and for the radiation-cooled arcjet, the value was 30.5%. Assuming frozen flow losses and nozzle losses are the same in both thruster, the difference should be due to anode losses. At that operating condition, 21.1% of the power was lost to the anode water-cooled anode, while 6.5% was measured for the radiation-cooled thruster using the radiant heat calorimeter. From the estimates made in the previous paragraphs, a value of 3% will be used to account for that heat lost to the anode and not measured by the calorimeter for the radiation-cooled arcjet. Consequently, the total anode losses for the hot-walled design were 9.5%. The difference in anode loss between the two thrusters was 11.6%. Multiplying this value by the nozzle efficiency gives the percentage of input electrical power converted to thrust in the radiation-cooled arcjet and not in the water-cooled thruster. The best available data for the nozzle efficiency are provided by the cold flow performance. Using the specific impulse value at 22.5 x 10^{-6} kg/s provided in Table III and eq. 4, the nozzle efficiency was estimated to be 0.7. The ideal specific impulse value used was 296 s, and was determined from the enthalpy of room temperature hydrogen[28] and the theory given by Jack[29]. Multiplying 11.6%, the difference in anode losses, by 0.7 gives 8.1%. The radiation-cooled thruster should convert 8.1% more of the electrical to thrust than the water-cooled design. The actual difference was 11.3%.

The same exercise was performed for the mixture data. To eliminate convective effects from the exhaust plume, a low facility background pressure operating point was chosen. The specific energy level was 30 MJ/kg at a flow rate of 49.0 x 10^{-6} kg/s. The radiation-cooled design converted 32.6% of the input electrical power to thrust power while the water-cooled thruster only converted 26.4%. The radiant heat calorimeter measured an anode loss of 6.8%. A value of 5% will be used to account for the heat not sensed by the calorimeter. The total anode loss measured by the water-cooled device was 25.6%. According to these data, 13.8% of the input electrical power was removed from the gas, by the water-cooled arcjet. Using the enthapy information in Ref. 28 for room temperature nitrogen and hydrogen and the theory in Ref 29, the ideal specific impulse was calculated to be 129 s, giving a nozzle efficiency of 0.8. Using that nozzle efficiency the predicted difference in electrical power converted to thrust power between the two thrusters is 11.0%. The actual value was 6.2%.

The greatest uncertainties in the above calculations are the estimates for the nozzle efficiency. The cold flow values were used and it is highly probable that with the arc on the viscous losses increase and the nozzle efficiencies are actually lower than estimated. Given all the uncertainties in the data and the assumptions made, the data for both propellants are in good agreement. In further studies improvements in closure should be seen by increased sensitivity in the measurements.

CONCLUDING REMARKS

The combination of performance data and information on anode losses data from both the water-cooled and radiation-cooled arcjets has provided insights into the energy deposition mechanisms of the arcjet. Cooling the arcjet nozzle walls results in a large degradation in performance. Regenerative heating of the propellant is eliminated and energy otherwise available for thrust is removed to a greater degree due to a larger temperature potential. To achieve

maximum performance of the arcjet the thruster should be run at the highest temperatures materials will allow.

All radiation-cooled designs will have some regenerative heating of the propellant as long as the nozzle temperature is greater than the incoming propellant temperature, which is the case for cryogenic fuels. The amount of energy recovered regeneratively is dependent on the thruster design. For the single-pass design tested in this study, 6-12% of the input electrical power was recovered regeneratively and converted to thrust for hydrogen and 3-6% for nitrogen/hydrogen mixtures. Room temperature simulated decomposed hydrazine was used, and the amount of regeneration for actual hydrazine decomposition products would be much less. It is clear that hydrogen, because of its high heat capacity, is a very promising propellant for a regenerative design. At a given specific energy, the fraction of input electrical power converted to thrust regeneratively is highly dependent on propellant flow rate and decreases with increasing flow rate.

The anode losses in the radiation-cooled hydrogen arcjet measured by the calorimeter ranged between 4% and 20% of the input electrical power for the flow rates and specific energy levels investigated. The fraction of energy lost was much less for operation on mixtures and was between 5% and 12% of the total input electrical power. These measured values of the anode loss do not take into account radiation losses from the inside surface of the nozzle, nor do they include heat conducted through the power cables and to the rear insulator. Those losses have been estimated to be 3% of the input electrical power for hydrogen operation and 5% for operation on nitrogen/hydrogen mixtures.

Clearly, significant power is available for regenerative heating. However, the amount of the recovered energy converted to thrust power depends on the nozzle efficiency. The maximum hydrogen cold flow nozzle efficiency was approximately 0.7 and probably decreases with the arc on. The combination of nozzle optimization and regenerative designs should lead to large gains in performance.

The fraction of power lost increased proportionally with current and at a given specific energy was inversely proportional to propellant flow rate. The decrease in anode losses is most probably due to a decrease in the anode fall voltage as the arc attachment region is pushed farther downstream.

A definite degradation in performance was noted when the facility background pressure was increased from nominally 0.2 Pa to 20 Pa. The change in efficiency was greater than could be accounted for by a simple pressure-area correction. An increase in anode losses was noted as the facility pressure was increased and when combined with a pressure correction may account for difference in efficiency. Since the differences in efficiency are only a few percent of the input electrical power, it is difficult to make quantitative statements about the increase in anode losses with facility pressure due to the uncertainties in this study. Further work needs to be conducted with greater sensitivity and a wider range of pressures to explain the phenomenon.

ACKNOWLEDGEMENTS

The authors wish to acknowledge Messrs. Fred K. Jent and Paul M. Switlyk for technical support to this project, especially for the fabrication of the radiant heat calorimeter.

REFERENCES

1. Wallner, L.E. and Czika, J. Jr.,"Arc-jet Thrustor for Space Propulsion," NASA TN D-2868, June 1965.

2. Yano, S. and Knowles, S.K.,"Simulated Flight Qualification Test of an Engineering Model Arcjet System," Proceedings of the 1989 JANNAF Propulsion Meeting, Cleveland, OH, 1989.

3. Curran, F.M. and Haag, T.W., "An Extended Life and Performance Test of a Low Power Arcjet," AIAA 88-3106, July 1988 (NASA TM-100942).

4. Haag, T.W. and Curran, F.M.,"Performance of a High Power Hydrogen Arcjet," AIAA 91-2226, to be presented at the 27th Joint Propulsion Conference, Sacramento, CA, June 1991.

5. Golz, T.M. et al.,"High Power Arcjet," 3rd progress report, NASA Grant NAGW-1736, IRS, Univ. of Stuttgart, Feb. 1991.

6 Deininger, W.D., et al., "30-kW Ammonia Arcjet Technology", JPL Publication 90-4, February 1990.

7. Morren, W.E. and Curran, F.M.," Preliminary Performance and Life Evaluation of a 2-kW-Class Arcjet," AIAA 91-2228, to be presented at the 27th Joint Propulsion Conference, Sacramento, CA, June 1991.

8. Curran, F.M. et al., "Medium Power Hydrogen Arcjet Performance," AIAA 91-227, to be presented at the 27th Joint Propulsion Conference, Sacramento, CA, June 1991.

9. Hamley, J.A. and Hill, G.M., "Power Electronics for Low Power Arcjets," AIAA 91-1991, to be presented at the 27th Joint Propulsion Conference, Sacramento, CA, June 1991.

10. Curran, F.M. and Sarmiento, C.J.,"Low Power Arcjet Performance Characterization," AIAA 90-2578, July 1990.

11. Curran, F.M., "An Experimental Study of the Energy Loss Mechanisms and Efficiency Considerations in the Low Power dc Arcjet," AIAA 85-2017, September 1985, (NASA TM 87123).

12. Cann, G.L., et. al.,"The Arc Jet," Proceedings, Symposium on Advanced Propulsion Concepts, 2nd, Oct. 7-9, 1959, U.S. GPO, Washington, D.C., 1960.

13. Stoner, W.A., "Investigation of a Low-Thrust Plasma Propulsion Device," Plasmadyne Corp., Santa Ana, CA, 1FR-021-1806, Feb. 1961.

14. Cobine, J.D., Gaseous Conductors, Dover Publications, New York, 1958.

15. Shih, K.T., et. al.,"Experimental Anode Heat-Transfer Studies in a Coaxial Arc Coonfiguration," AIAA Journal, Vol. 6, No. 8, Aug. 1968, pp. 1482-1487.

16. Knowles, S.C., et al.,"Performance Characterization of a Low Power Hydrazine Arcjet," AIAA 87-1057, May 1987.

17. John, R.R. et al.,"Arc Jet Engine Performance: Experiment and Theory," AIAA Journal, Vol. 1, No. 11, Nov. 1963, pp. 2517-2524.

18. Haag, T.W. and Curran, F.M., "Arcjet Starting Reliability: A Multistart Test," AIAA 87-1061, May 1987 (NASA TM 89867).

19. Gruber, R.P., et al.,"5-kW Arcjet Power Electronics," AIAA 89-2725, July 1989, (NASA TM 102108).

20. Zube, D. and Myers, R.M., "Nonequilibrium in a Low Power Arcjet Nozzle," AIAA 91-2113, to be presented at the 27th Joint Propulsion Conference, Sacramento, CA, June 1991.

21. Rieck, G.D., Tungsten and Its Compounds, Pergamon, Oxford, 1967, p. 27.

22. Curran, F.M. and Manzella, D.H., "The Effects of Electrode Configuration on Arcjet Performance," AIAA 89-2722. (NASA 102346)

23. Sankovic, J.M., "Investigation of the Arcjet Plume Near Field Using Electrostatic Probes," Proceedings of the 1990 JANNAF Propulsion Meeting, Anaheim, CA, Oct. 1990. (NASA TM-103638).

24. Curran, F.M. et al.,"Performance Characterization of a Segmented Anode Arcjet Thruster," AIAA 90-2582, July 1990.

25. Manzella, et al., "Effect of Ambient Pressure on the Performance of a Resistojet," J. of Propulsion and Power, Vol .5 No. 4, July 1989, pp. 452-456.

26. Siegel R.,and Howell, J.R. Radiation Heat Transfer, Hemisphere, New York, 1981.

27. Bien, D.D.,"Configuration Factors for Thermal Radiation for Isothermal Inner Walls of Cones and Cylinders," J. of Spacecraft and Rockets, Vol. 3, No. 1., pp. 155-156, 1966.

28. Van Wylen, G.J. and Sonntag, R.E., Fundamentals of Classical Thermodynamics, 3rd ed., John Wiley and Sons, 1986.

29. Jack, John R.,"Theoretical Performance of Propellants Suitable for Electrothermal Jet Engines," NASA TN D-682, 1961.

Table I. Hydrogen, radiation-cooled arcjet performance

I A	V V	P_e W	m_p kg/s x10^6	P_e/m_p J/kg x10^{-6}	F mN	p kPa	I_{sp} s	f_t %	P_r W	f_r %	p_b Pa
35.0	112.5	3940	22.5	175	234	396	1060	29.4	227	5.8	45.3
30.0	114.3	3430	22.5	152	223	379	1010	30.4	205	6.0	45.3
25.0	115.9	2900	22.5	129	210	359	949	31.4	187	6.5	45.3
25.0	118.3	2960	22.5	131	211	334	956	31.4	194	6.6	45.3
20.0	117.1	2340	22.5	104	190	330	864	31.7	152	6.5	45.3
15.0	119.3	1790	22.5	80	169	299	765	31.8	108	6.0	45.3
35.0	98.4	3440	15.0	230	162	312	1100	24.2	248	7.2	30.7
30.0	100.8	3020	15.0	202	155	296	1060	25.3	245	8.1	30.7
25.0	102.2	2560	15.0	170	147	277	1000	26.7	212	8.3	30.7
20.0	103.9	2080	15.0	139	136	254	929	28.1	190	9.1	30.7
15.0	106.7	1600	15.0	107	124	230	838	29.2	157	9.8	30.7
25.0	88.4	2210	10.0	221	95	215	971	19.4	224	10.1	20.1
20.0	90.4	1810	10.0	181	90	194	917	21.0	206	11.4	20.1
15.0	93.1	1400	10.0	140	82	177	840	22.5	165	11.8	20.1

Table II. Hydrogen, water-cooled arcjet performance

I A	V V	P_e W	m_p kg/s x10^6	P_e/m_p J/kg x10^{-6}	F mN	p kPa	I_{sp} s	f_t %	p_b Pa
35.0	102.2	3580	22.5	159	184	239	835	19.3	44.9
30.0	102.0	3060	22.5	136	171	229	775	19.1	44.9
25.0	104.0	2600	22.5	116	161	222	730	19.7	44.9
20.0	106.1	2120	22.5	94	148	213	670	19.8	44.9
15.0	110.9	1660	22.5	74	132	203	601	19.7	44.9
35.0	86.3	3020	15.0	201	124	193	841	15.6	31.3
30.0	92.1	2760	15.0	184	121	184	821	16.2	31.3
25.0	92.5	2310	15.0	154	113	176	766	16.6	31.3
20.0	95.0	1900	15.0	127	105	164	712	17.2	31.3

Table III. Hydrogen cold gas performance

m_p kg/s x10^6	F mN	p kPa	I_{sp} s	p_b Pa
22.5	54	159	244	44.9
15.0	34	111	233	31.3
10.0	23	77.7	228	22.0

Table IV. Radiant heat calorimetry data for a hydrogen arcjet

I A	V V	P_e W	m_p kg/s x10^6	P_e/m_p J/kg x10^{-6}	ΔT K	m_w kg/s x10^3	P_{cal} W	f_{cal} %
40.0	108.2	4330	22.5	192	13.0	6.4	349	8.1
35.0	109.1	3820	22.5	170	10.7	6.2	279	7.3
30.0	109.7	3290	22.5	146	8.1	6.2	210	6.4
25.0	111.0	2780	22.5	123	5.9	6.1	151	5.4
20.0	111.8	2240	22.5	99	4.3	6.0	107	4.8
15.0	113.8	1710	22.5	76	2.7	6.0	68	4.0
35.0	93.7	3280	15.0	219	17.1	6.7	476	14.5
30.0	96.7	2900	15.0	193	13.8	6.4	365	12.6
30.0	97.0	2910	15.0	194	9.2	9.4	361	12.4
30.0	97.0	2910	15.0	194	12.7	6.9	364	12.5
25.0	95.9	2400	15.0	160	10.5	6.4	278	11.6
20.0	97.9	1960	15.0	131	6.8	6.4	180	9.2
15.0	99.4	1490	15.0	99	3.8	6.4	100	6.7
25.0	81.9	2050	10.0	205	13.9	6.4	370	18.1
20.0	85.1	1700	10.0	170	10.3	6.2	269	15.8
15.0	87.7	1320	10.0	132	6.3	6.2	165	12.5

Table V. Calorimetry data for a hydrogen, water-cooled arcjet

I A	V V	P_e W	m_p kg/s x10^6	P_e/m_p J/kg x10^{-6}	ΔT K	m_w kg/s x10^3	P_{cal} W	f_{cal} %
35.0	102.2	3580	22.5	159	15.3	12.1	770	21.5
30.0	102.0	3060	22.5	136	14.1	10.8	630	20.6
25.0	104.0	2600	22.5	116	10.7	10.8	483	18.6
20.0	106.1	2120	22.5	94	7.9	10.6	349	16.5
15.0	110.9	1660	22.5	74	6.5	8.7	236	14.2
35.0	86.3	3020	15.0	201	20.0	11.7	971	32.2
30.0	92.1	2760	15.0	184	17.9	11.7	869	31.4
25.0	92.5	2310	15.0	154	14.6	11.4	696	30.1
20.0	95.0	1900	15.0	127	10.4	11.4	495	26.1

Table VI. 1:2 nitrogen/hydrogen mixtures, radiation-cooled arcjet performance at high facility background pressures

I A	V V	P_e W	m_p kg/s x10^6	P_e/m_p J/kg x10^{-6}	F mN	p kPa	I_{sp} s	f_t %	P_r W	f_r %	p_b Pa
22.0	102.0	2240	61.7	36.4	301	416	497	31.1	69	3.1	24.5
18.0	104.6	1880	61.7	30.5	277	389	458	31.1	59	3.1	24.5
14.0	110.3	1540	61.7	25.0	251	363	415	30.7	49	3.2	24.5
10.0	120.7	1210	61.7	19.6	222	333	366	30.0	38	3.1	24.5
18.0	98.1	1770	49.0	36.0	235	344	490	30.3	75	4.2	20.3
16.0	100.4	1610	49.0	32.8	225	329	468	30.2	75	4.6	20.3
14.0	103.3	1450	49.0	29.5	214	316	445	30.1	67	4.6	20.3
12.0	107.0	1280	49.0	26.2	201	300	419	29.8	59	4.6	20.3
10.0	111.5	1120	49.0	22.8	190	287	395	30.1	48	4.3	20.3
8.0	120.6	965	49.0	19.7	176	270	366	29.4	41	4.2	20.3
14.0	92.4	1290	36.4	35.5	165	253	462	27.3	68	5.3	15.7
12.0	96.3	1160	36.4	31.7	157	246	441	27.5	64	5.5	15.7
10.0	101.4	1010	36.4	27.9	148	231	416	27.7	54	5.4	15.7
8.0	107.6	861	36.4	23.6	136	217	382	27.2	47	5.5	15.7

Table VII. 1:2 nitrogen/hydrogen mixtures, radiation-cooled arcjet performance at low facility background pressures

I A	V V	P_e W	m_p kg/s x10^6	P_e/m_p J/kg x10^{-6}	F mN	p kPa	I_{sp} s	f_t %	P_r W	f_r %	p_b Pa
18.0	99.3	1790	49.0	36.5	247	352	514	33.0	72	4.0	0.23
16.0	101.5	1620	49.0	33.1	235	339	490	32.8	72	4.4	0.23
14.0	104.5	1460	49.0	29.9	224	321	465	32.6	64	4.4	0.23
12.0	107.9	1300	49.0	26.4	211	305	438	32.4	58	4.5	0.23
10.0	113.4	1130	49.0	23.1	196	289	408	31.8	49	4.3	0.23
10.0	112.4	1120	49.0	22.9	197	290	410	32.4	50	4.5	0.23
8.0	121.8	974	49.0	19.9	183	--	382	32.0	44	4.5	0.23
14.0	93.3	1310	36.4	35.9	174	259	489	30.2	77	5.9	0.15
12.0	97.7	1170	36.4	32.2	166	250	465	30.2	73	6.2	0.15
10.0	103.1	1030	36.4	28.3	157	239	439	30.4	65	6.3	0.15
8.0	110.4	883	36.4	24.3	147	227	411	30.8	57	6.5	0.15

Table VIII. 1:2 nitrogen/hydrogen mixtures, water-cooled arcjet performance at high facility background pressures

I A	V V	P_e W	m_p kg/s x10^6	P_e/m_p J/kg x10^{-6}	F mN	p kPa	I_{sp} s	f_t %	p_b Pa
22.0	95.4	2100	61.7	34.0	270	298	446	26.3	25.7
18.0	100.0	1800	61.7	29.2	248	284	410	25.6	25.7
14.0	110.4	1550	61.7	25.1	225	271	370	23.9	25.7
14.0	107.9	1510	61.7	24.5	221	271	365	23.7	25.7
10.0	119.1	1190	61.7	19.3	197	257	325	23.2	25.7
18.0	90.1	1620	49.0	33.1	204	243	424	24.4	21.7
16.0	92.0	1470	49.0	30.0	196	234	408	24.6	21.7
14.0	95.5	1340	49.0	27.3	185	228	385	23.9	21.7
12.0	99.5	1190	49.0	24.4	175	238	364	23.7	21.7
10.0	106.3	1060	49.0	21.7	165	212	343	23.4	21.7

Table IX. 1:2 nitrogen/hydrogen mixtures ,water-cooled arcjet performance at low facility background pressures

I A	V V	P_e W	m_p kg/s x10^6	P_e/m_p J/kg x10^{-6}	F mN	p kPa	I_{sp} s	f_t %	p_b Pa
18.0	90.1	1622	49.0	33.1	214	240	445	26.8	0.29
16.0	92.4	1480	49.0	30.2	204	232	424	26.4	0.29
14.0	95.5	1340	49.0	27.3	193	225	402	26.1	0.29
12.0	99.7	1200	49.0	24.4	182	218	380	25.7	0.29
10.0	106.2	1060	49.0	21.7	173	212	359	25.5	0.29

Table X. 1:2 nitrogen/hydrogen mixtures cold gas performance at high and low facility background pressures

m_p kg/s x10^6	F mN	p kPa	I_{sp} s	p_b Pa
61.7	68.4	191.1	113	26.3
49.0	54.0	152.4	112	21.6
36.4	39.4	115.2	110	16.9
49.0	55.5	152.7	116	0.29
36.4	41.5	115.2	116	0.13

Table XI. Calorimetry data for a water-cooled arcjet operating at high facility background pressures on 1:2 nitrogen/hydrogen mixtures

I A	V V	P_e W	m_p kg/s x10^6	P_e/m_p J/kg x10^{-6}	ΔT K	m_w kg/s x10^3	P_{cal} W	f_{cal} %
22.0	95.4	2100	61.7	34.0	15.2	7.7	487	23.2
18.0	100.0	1800	61.7	29.2	12.8	7.5	399	22.2
14.0	110.4	1550	61.7	25.1	12.6	7.3	384	24.8
14.0	107.9	1510	61.7	24.5	12.3	7.2	369	24.4
10.0	119.1	1190	61.7	19.3	9.4	7.2	282	23.7
18.0	90.1	1620	49.0	33.1	15.3	7.0	447	27.6
16.0	92.0	1470	49.0	30.0	12.8	7.1	380	25.8
14.0	95.5	1340	49.0	27.3	11.3	7.3	345	25.8
12.0	99.5	1190	49.0	24.4	9.9	7.0	289	24.2
10.0	106.3	1060	49.0	21.7	8.1	7.2	243	22.9

Table XII. Calorimetry data for a water-cooled arcjet operating at low facility background pressures on 1:2 nitrogen/hydrogen mixtures

I A	V V	P_e W	m_p kg/s x10^6	P_e/m_p J/kg x10^{-6}	ΔT K	m_w kg/s x10^3	P_{cal} W	f_{cal} %
18.0	90.1	1622	49.10	33.1	15.7	6.5	424	26.1
16.0	92.4	1480	49.0	30.2	13.4	6.8	380	25.7
14.0	95.5	1340	49.0	27.3	11.9	6.6	326	24.4
12.0	99.7	1200	49.0	24.4	9.9	6.7	276	23.1
10.0	106.2	1060	49.0	21.7	9.3	6.0	231	21.7

Table XIII. Radiant heat calorimetry data for an arcjet operating at high facility background pressures on 1:2 nitrogen/hydrogen mixtures

I A	V V	P_e W	m_p kg/s x10^6	P_e/m_p J/kg x10^{-6}	ΔT K	m_w kg/s x10^3	P_{cal} W	f_{cal} %
22.0	100.1	2200	61.7	35.7	7.9	5.7	186	8.5
20.0	101.2	2020	61.7	32.8	7.1	5.7	168	8.3
18.0	102.2	1840	61.7	29.8	6.0	5.6	141	7.6
16.0	103.6	1660	61.7	26.9	5.2	5.6	120	7.3
14.0	106.1	1490	61.7	24.1	3.8	5.8	91	6.1
12.0	110.1	1320	61.7	21.4	3.2	5.7	76	5.8
10.0	116.5	1170	61.7	18.9	3.0	5.7	71	6.1
8.0	125.9	1010	61.7	16.3	2.4	5.7	56	5.6
18.0	94.9	1710	49.0	34.9	7.2	5.6	170	9.9
16.0	96.3	1540	49.0	31.4	6.1	5.8	148	9.6
14.0	98.4	1380	49.0	28.1	5.2	5.7	122	8.8
12.0	101.9	1220	49.0	25.0	4.2	5.8	101	8.3
10.0	107.2	1070	49.0	21.9	3.4	5.7	82	7.6
8.0	114.5	916	49.0	18.7	2.8	5.6	65	7.1
14.0	87.7	1230	36.4	33.7	6.1	5.6	14	11.7
12.0	91.1	1090	36.4	30.0	5.3	5.6	124	11.3
10.0	96.0	960	36.4	26.4	4.3	5.8	103	10.7
8.0	103.3	826	36.4	22.7	3.3	5.8	79	9.6
6.0	114.7	688	36.4	18.9	2.6	5.8	63	9.2

Table XIV. Radiant heat calorimetry data for an arcjet operating at low facility background pressures on 1:2 nitrogen/hydrogen mixtures

I A	V V	P_e W	m_p kg/s x10^6	P_e/m_p J/kg x10^{-6}	ΔT K	m_w kg/s x10^3	P_{cal} W	f_{cal} %
18.0	95.8	1720	49.0	35.2	5.6	5.7	134	7.8
16.0	97.4	1560	49.0	31.8	4.4	6.0	111	7.2
14.0	99.4	1390	49.0	28.4	3.9	5.5	89	6.4
12.0	103.1	1240	49.0	25.2	3.2	5.5	72	5.8
10.0	108.5	1090	49..0	22.1	2.3	5.8	56	5.1
8.0	116.3	930	49.0	19.0	1.9	5.8	47	5.1
14.0	89.1	1250	36.4	34.3	4.9	5.7	117	9.4
12.0	92.7	1110	36.4	30.6	4.1	5.5	94	8.4
10.0	97.7	977	36.4	26.8	3.3	5.6	76	7.8
8.0	105.0	840	36.4	23.1	2.4	5.5	56	6.7

Table XV. Power radiated from nozzle surface to space

T K	ϵ	Q_a W
1000	0.10	1
1500	0.15	5
2000	0.20	19
2500	0.25	57
3000	0.30	142

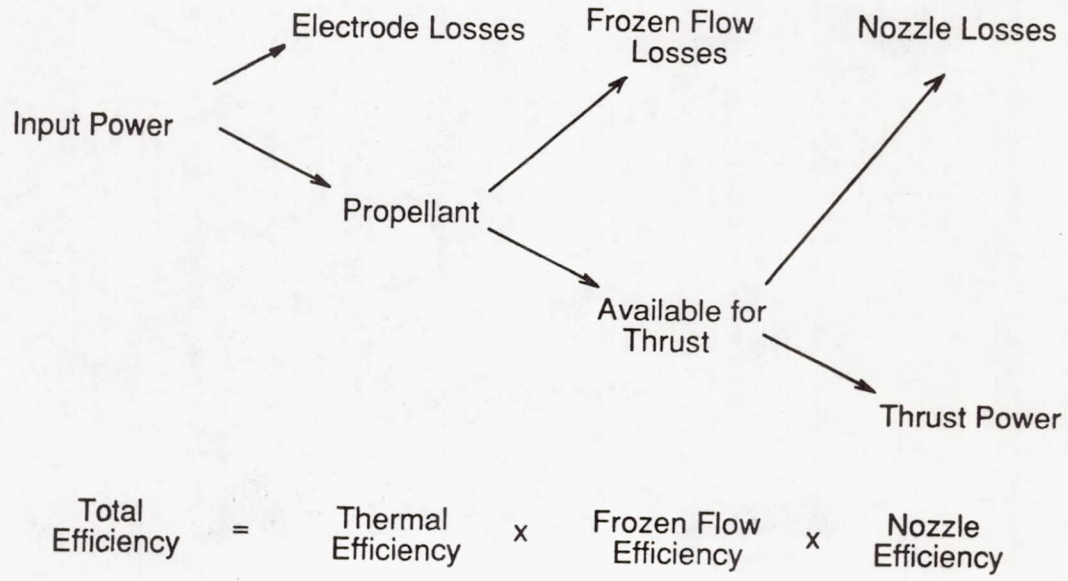

Figure 1. Energy deposition in an arcjet.

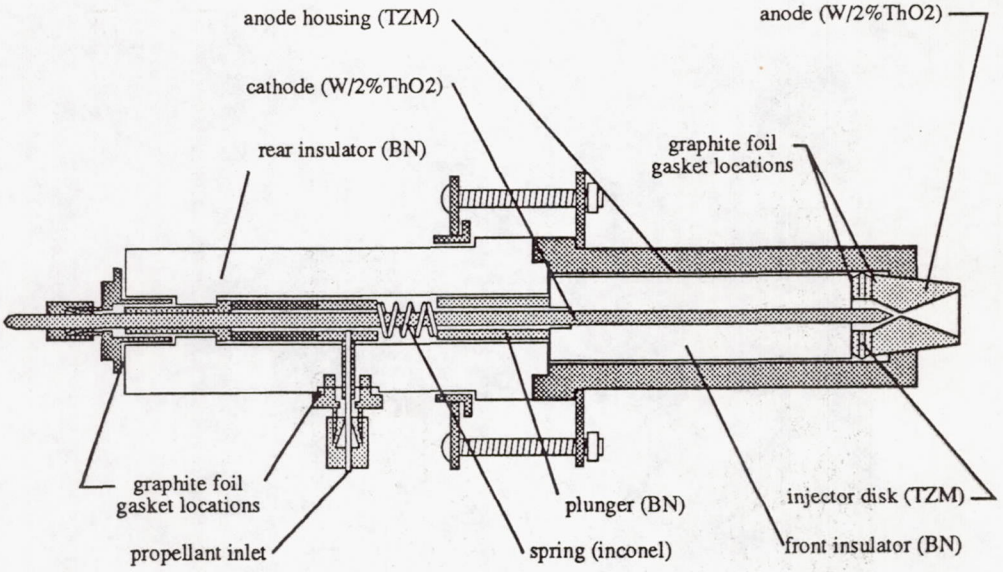

Figure 2. Schematic of radiation-cooled arcjet.

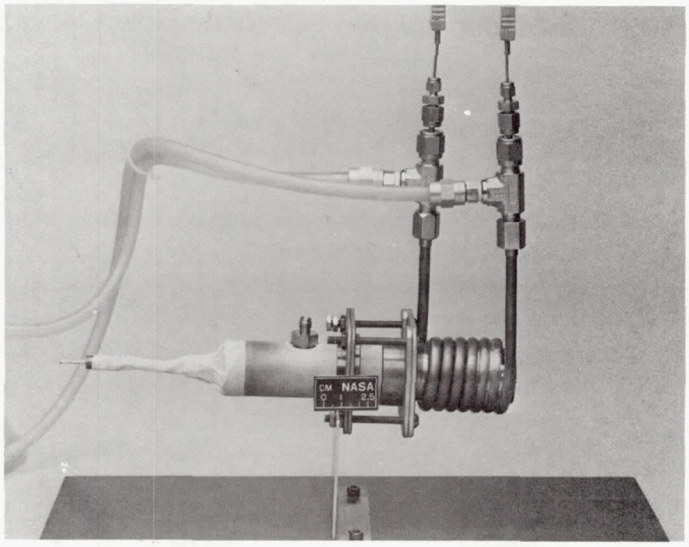

(a) Side-view of thruster.

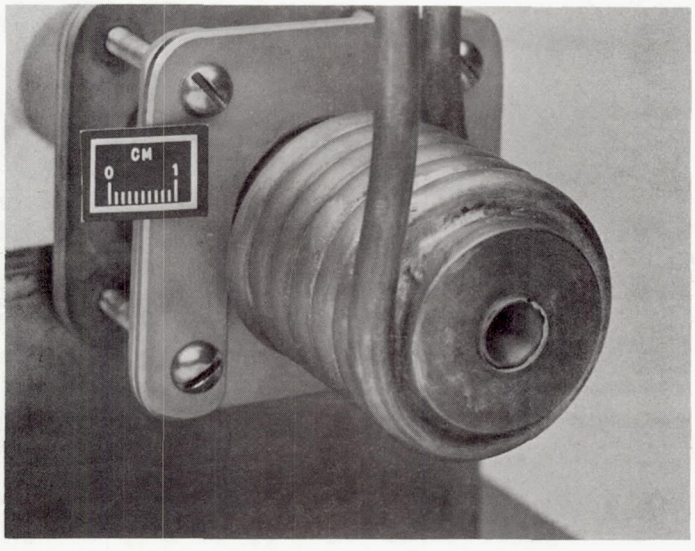

(b) Closeup of anode.

Figure 3.—Water-cooled arcjet.

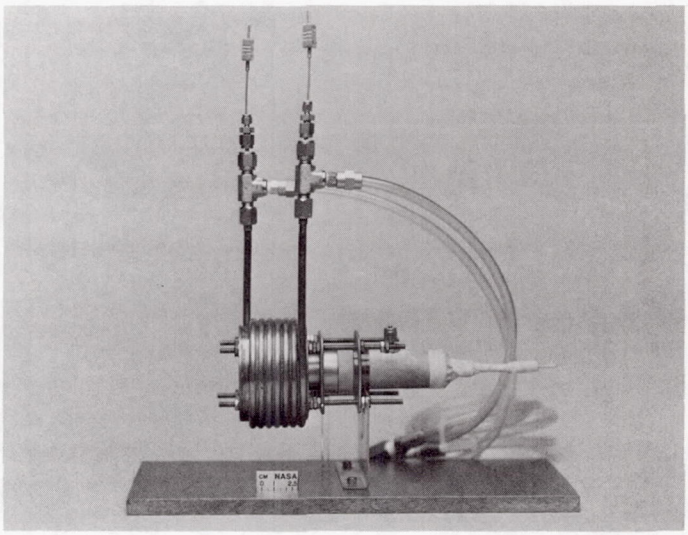

(a) Radiant heat calorimeter mounted on arcjet.

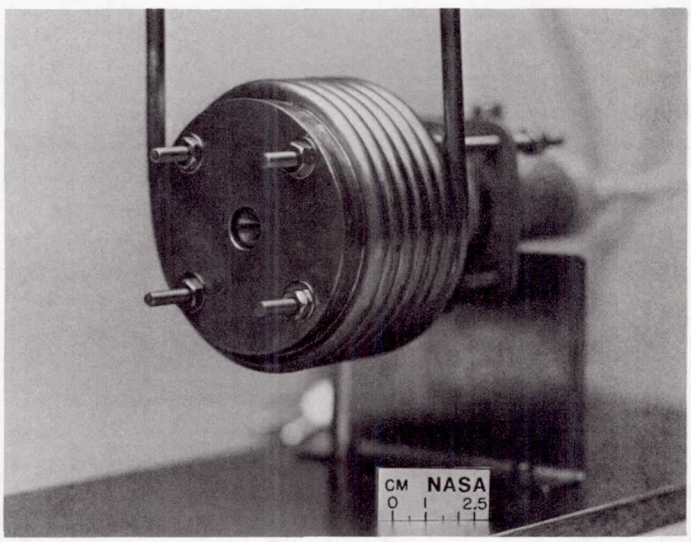

(b) Closeup of calorimeter.

Figure 4.—Radiant heat calorimeter.

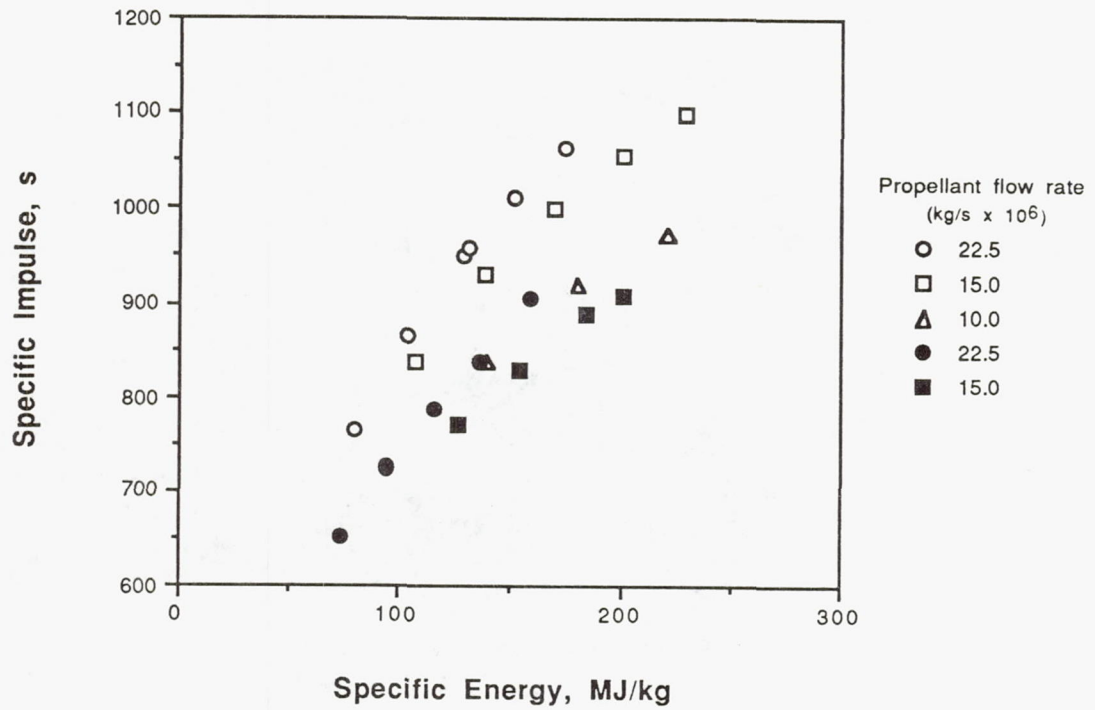

Figure 5. Specific impulse versus specific energy at various hydrogen propellant flow rates. Open symbols represent radiation-cooled thruster and closed represent water-cooled thruster.

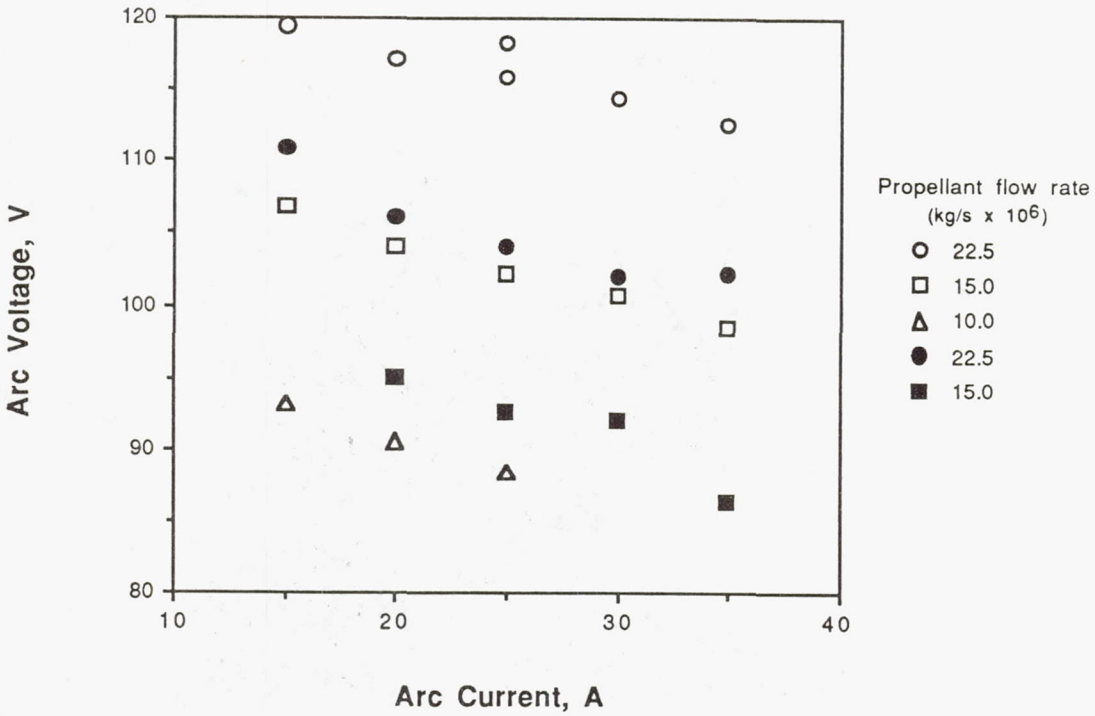

Figure 6. Arc voltage versus arc current at various hydrogen propellant flow rates. Open symbols represent radiation-cooled thruster and closed represent water-cooled thruster.

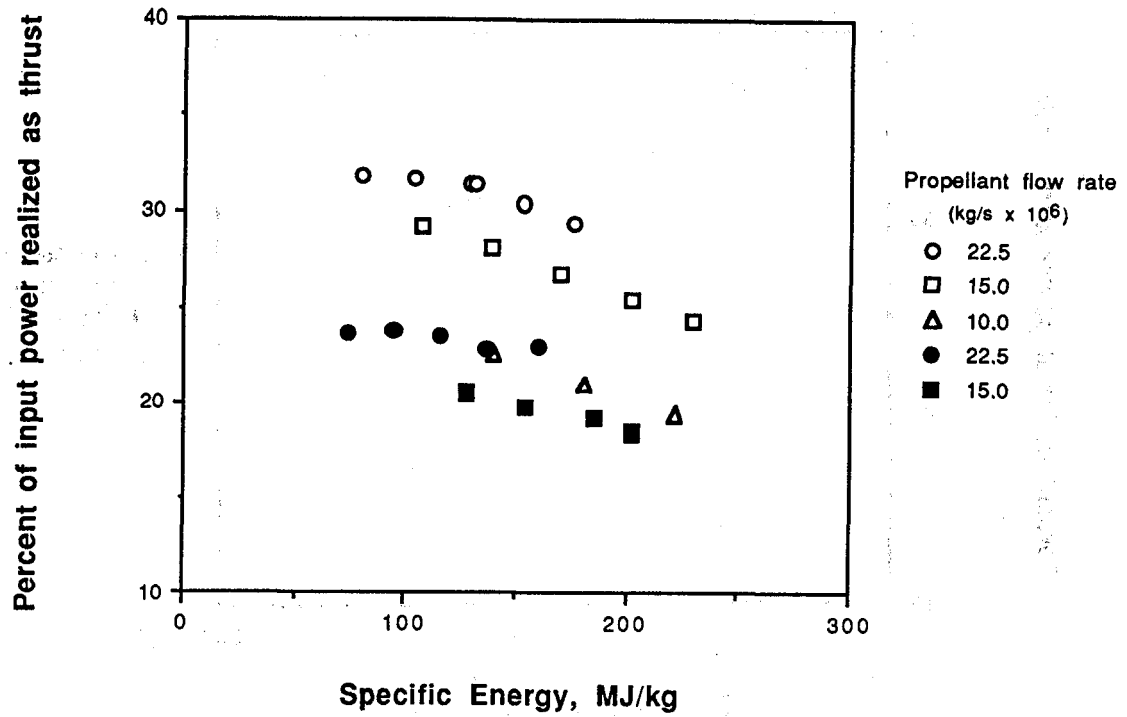

Figure 7. Percent of input electrical power realized as thrust as a function of specific energy and hydrogen propellant flow rate. Open symbols represent radiation-cooled thruster and closed represent water-cooled thruster.

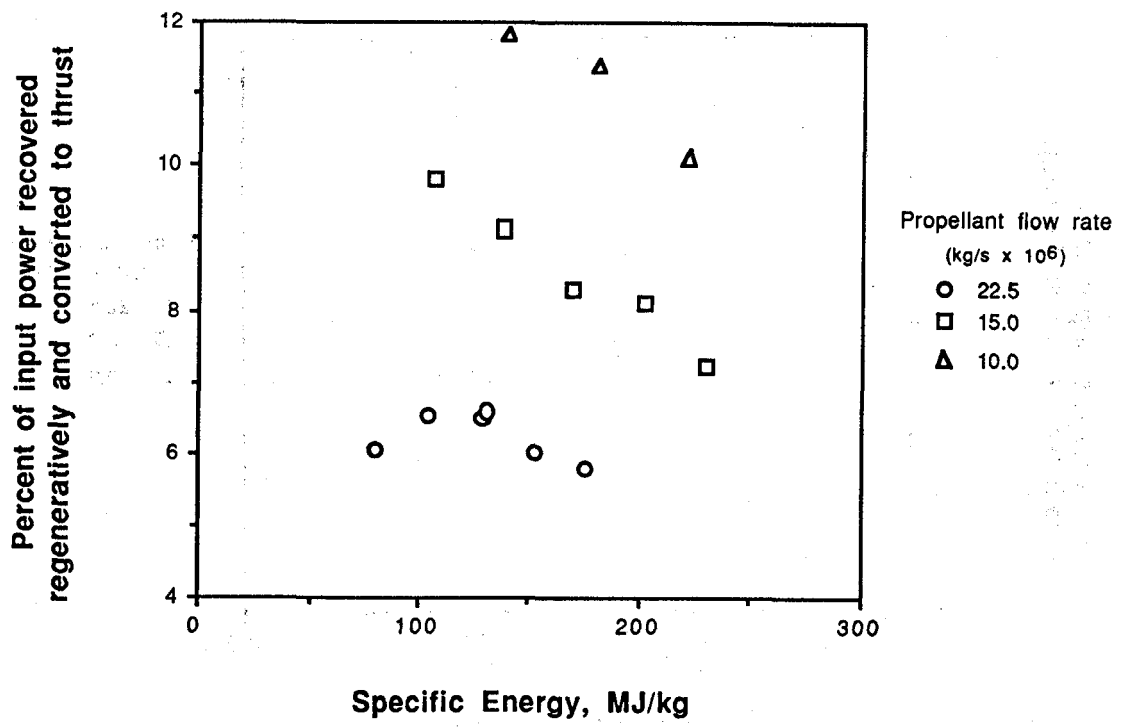

Figure 8. Percent of input electrical power recovered regeneratively and converted to thrust as a function of specific energy and hydrogen propellant flow rate.

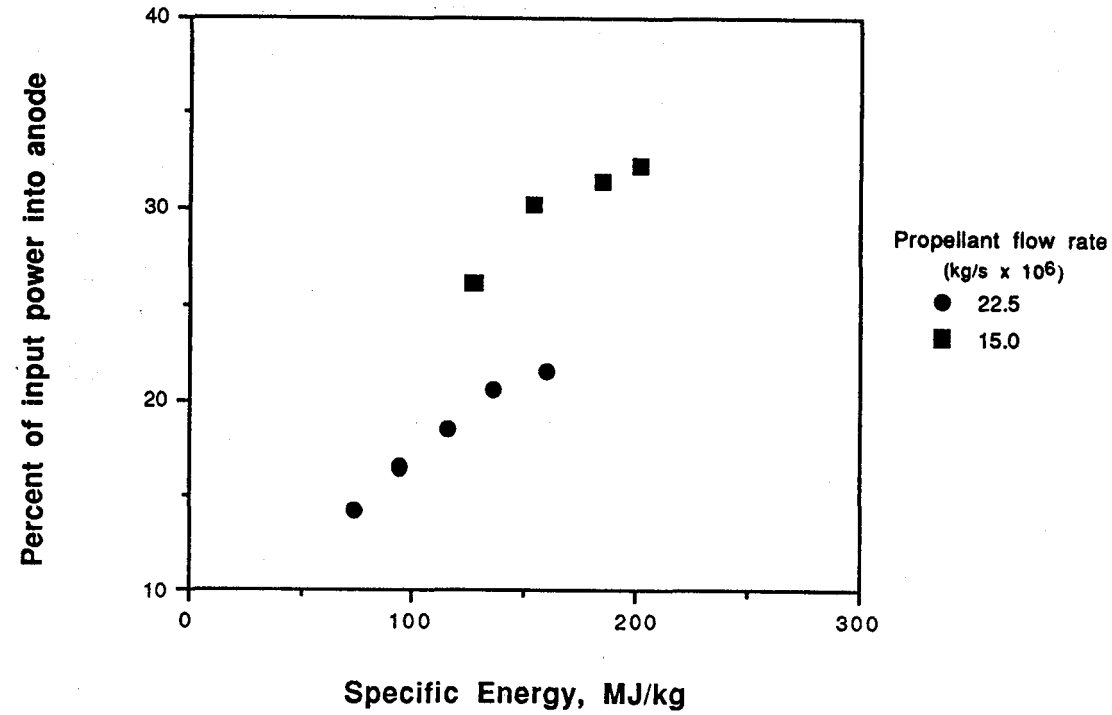

Figure 9. Percent of input electrical power deposited into water-cooled anode versus specific energy at different hydrogen propellant flow rates.

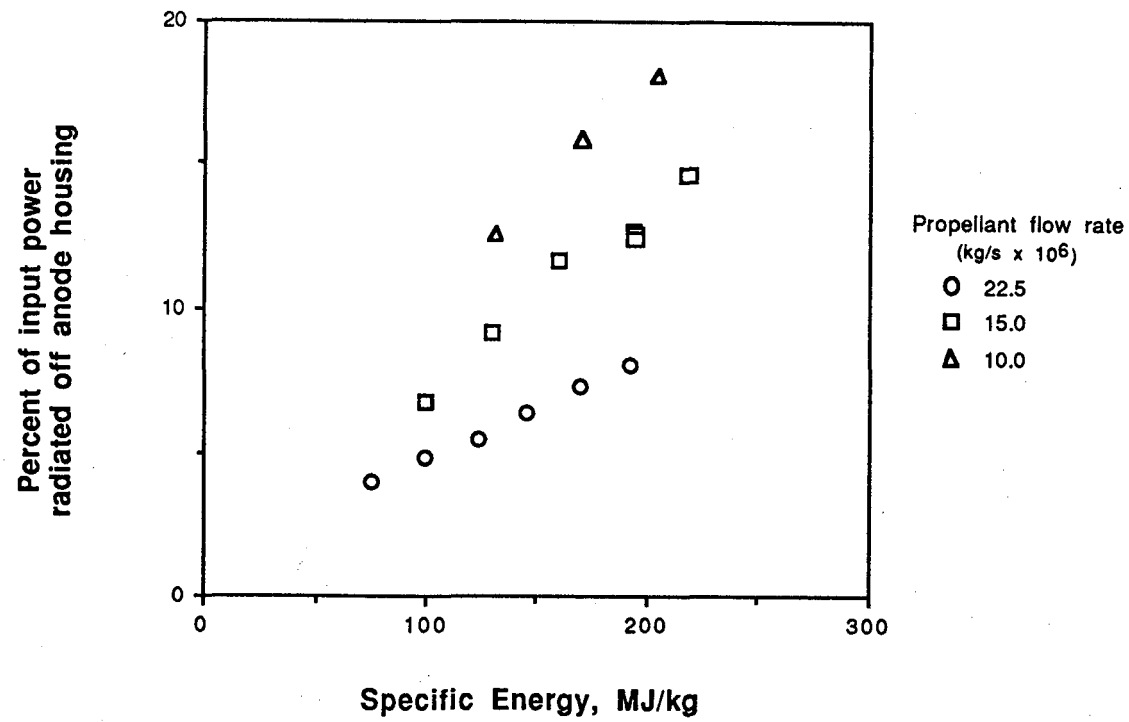

Figure 10. Percent of input electrical power radiated off anode housing versus specific energy at various hydrogen propellant flow rates.

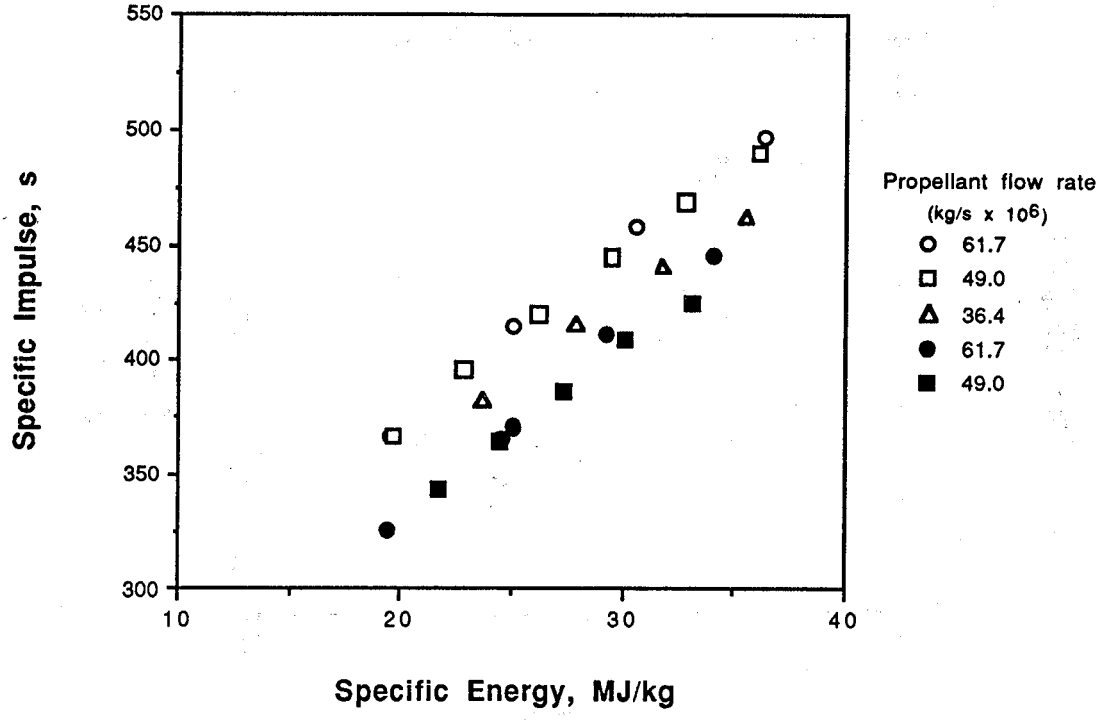

Figure 11. Specific impulse versus specific energy at various 1:2 nitrogen/hydrogen mixture propellant flow rates at facility background pressures nominally 20 Pa. Open symbols represent radiation-cooled thruster, and closed represent water-cooled thruster.

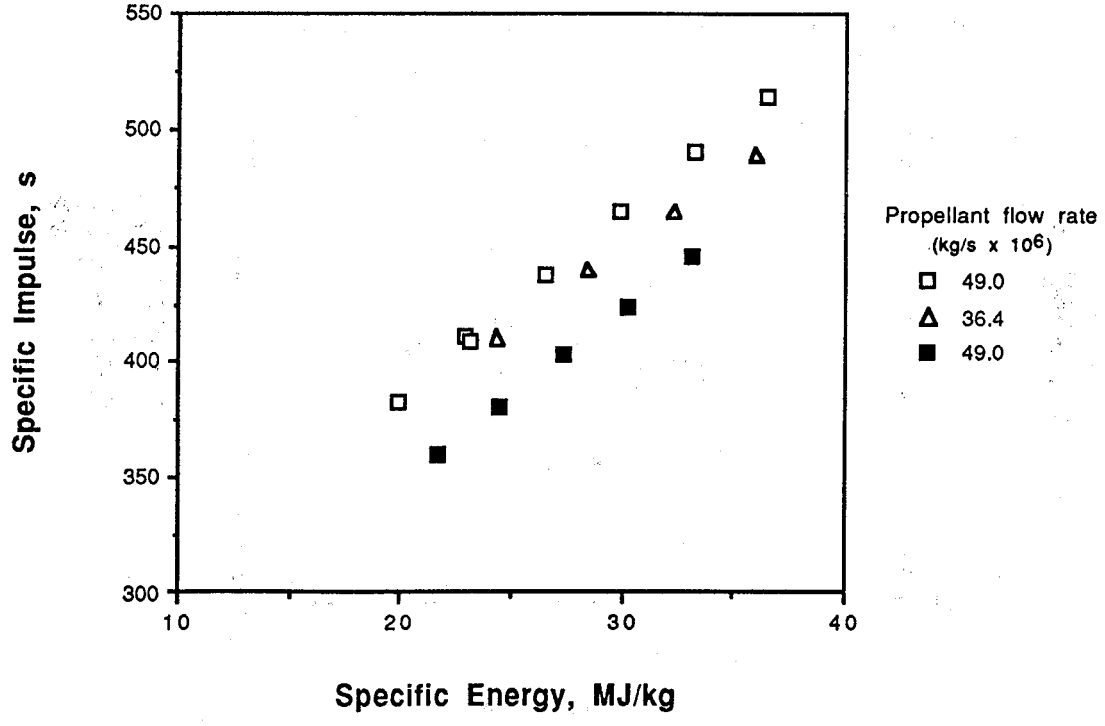

Figure 12. Specific impulse versus specific energy at various 1:2 nitrogen/hydrogen mixture propellant flow rates at facility background pressures nominally 0.2 Pa. Open symbols represent radiation-cooled thruster, and closed represent water-cooled thruster.

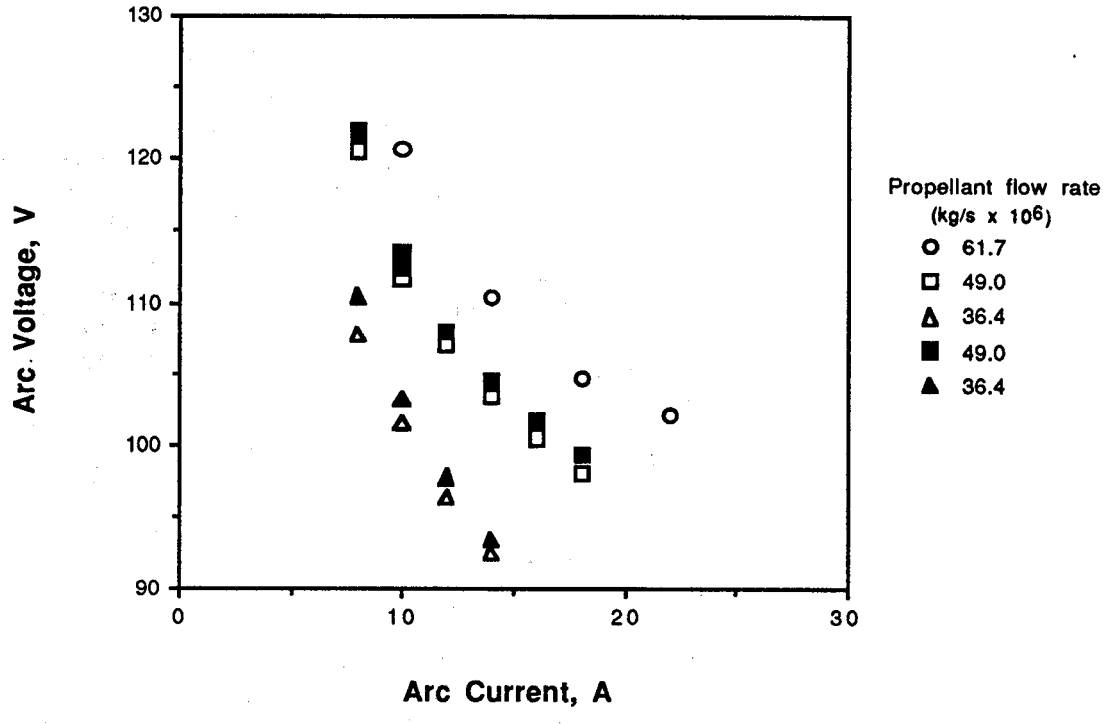

Figure 13. Arc voltage versus arc current at various 1:2 nitrogen/hydrogen mixture propellant flow rates for the radiation-cooled thruster. Open symbols represent a facility background pressure nominally 20 Pa, and closed represent a pressure nominally 0.2 Pa.

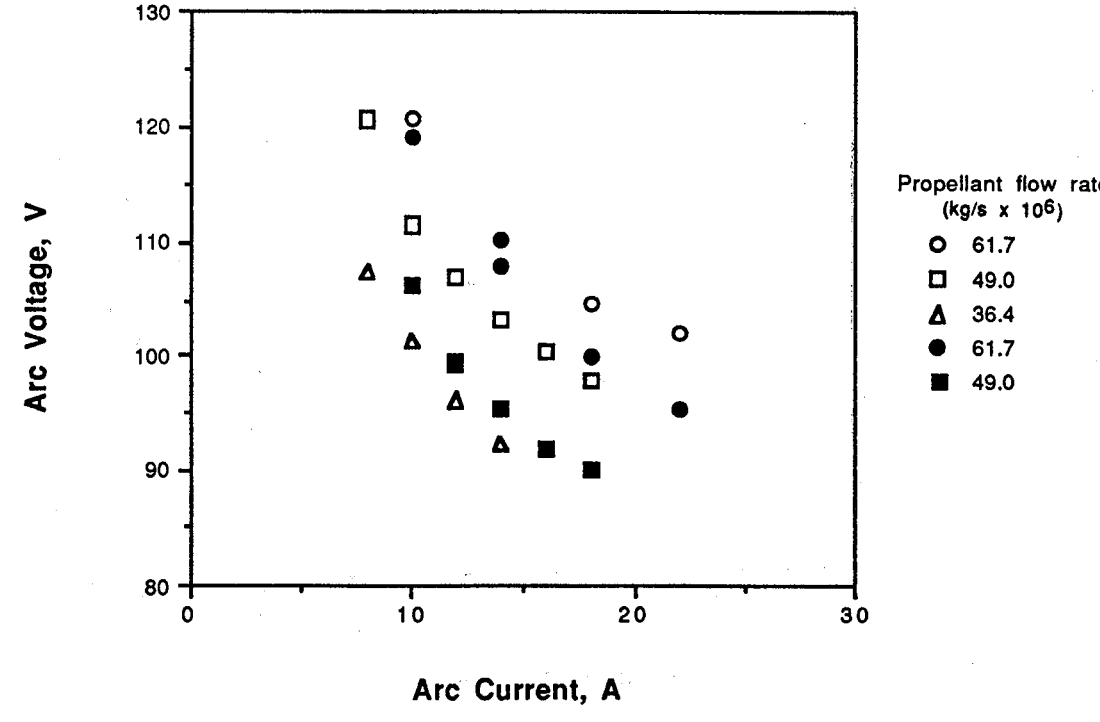

Figure 14. Arc voltage versus arc current at various 1:2 nitrogen/hydrogen mixture propellant flow rates for operation at a nominal facility background pressure of 20 Pa. Open symbols represent radiation-cooled arcjet, and closed represent water-cooled arcjet.

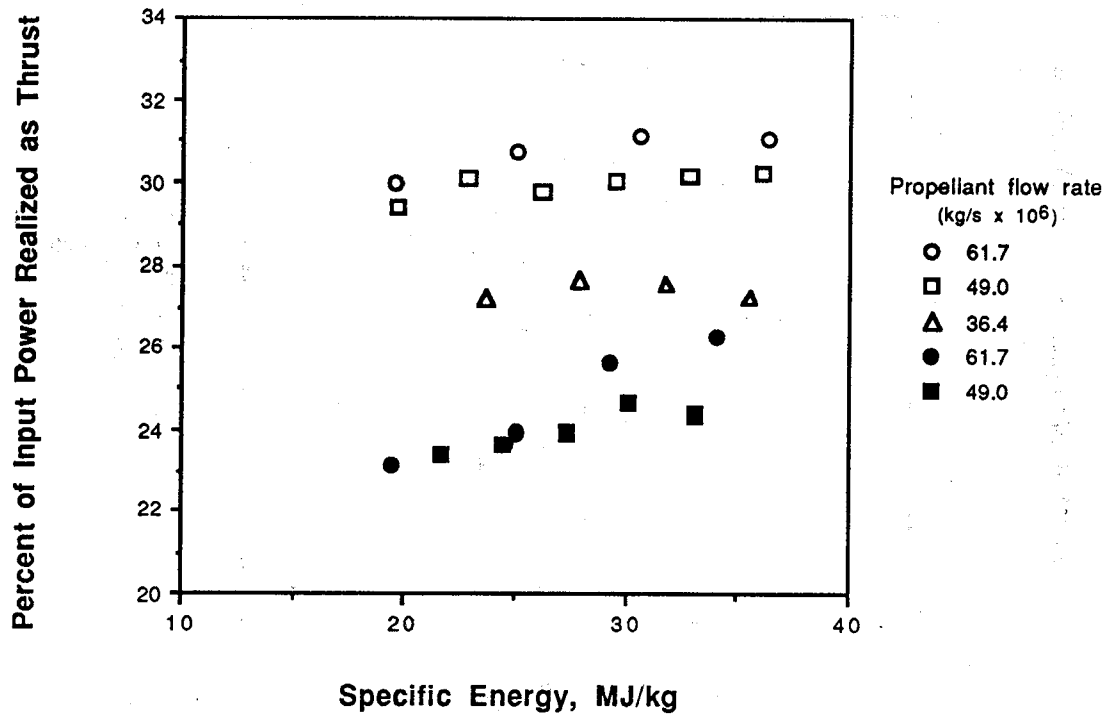

Figure 15. Percent of input power realized as thrust versus specific energy for1:2 nitrogen/hydrogen mixture operation at a nominal facility background pressure of 20 Pa. Open symbols represent radiation-cooled arcjet, and closed represent water-cooled arcjet.

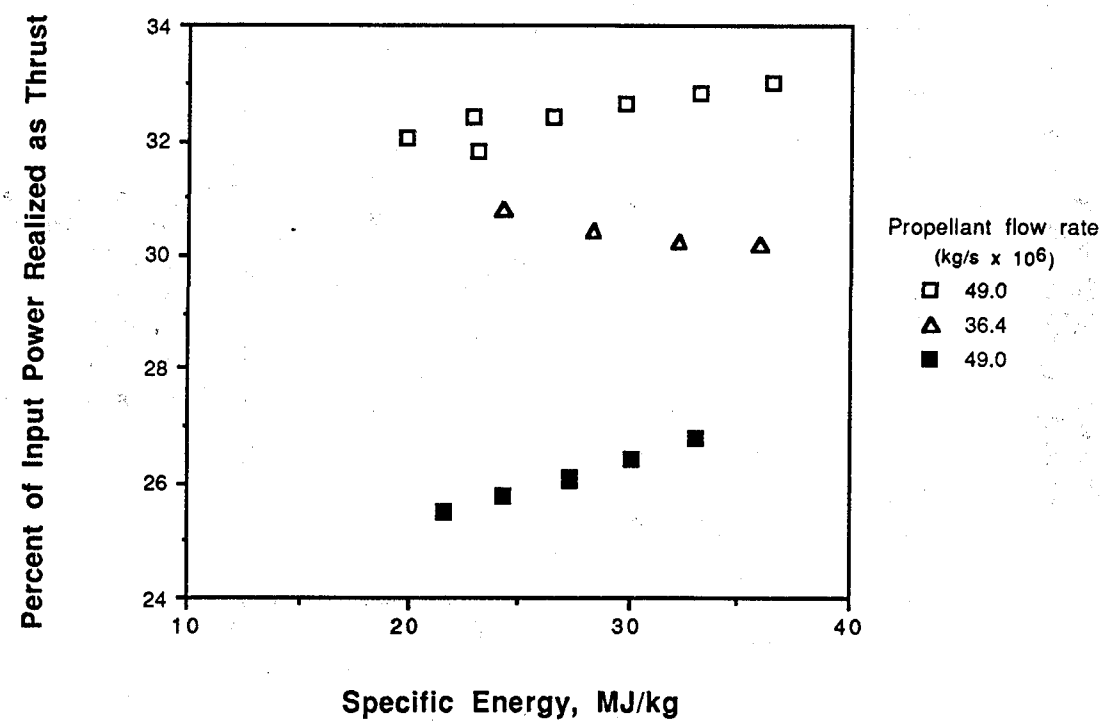

Figure 16. Percent of input power realized as thrust versus specific energy for 1:2 nitrogen/hydrogen mixture operation at a nominal facility background pressure of 0.20 Pa. Open symbols represent radiation-cooled arcjet, and closed represent water-cooled arcjet.

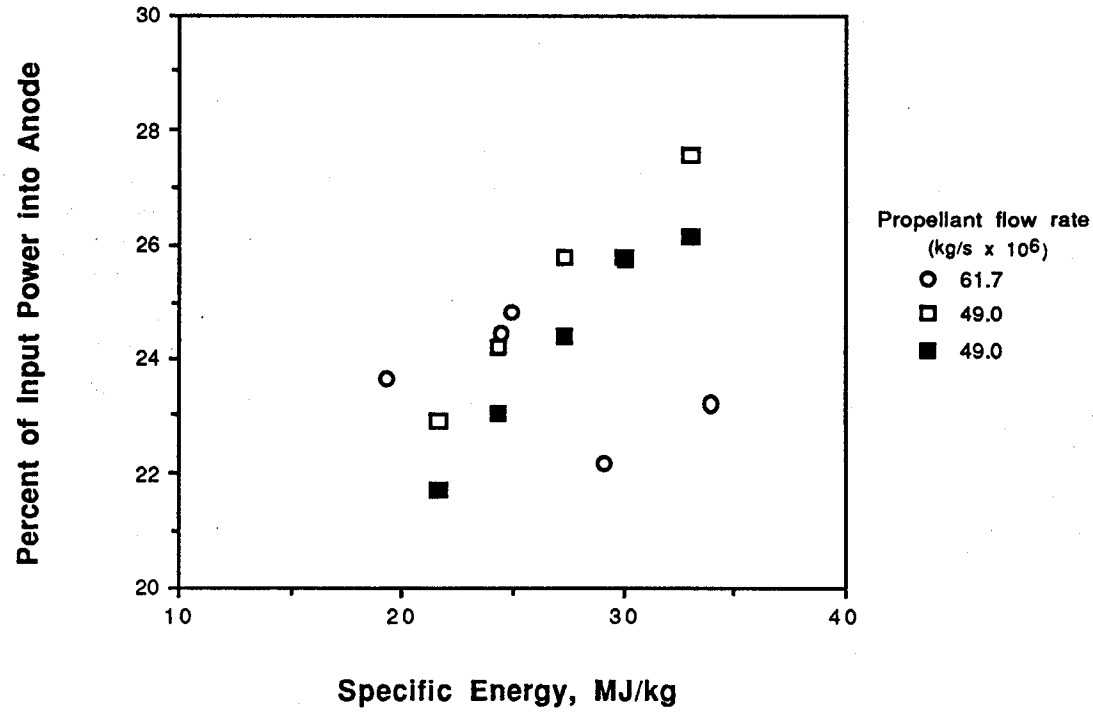

Figure 17. Percent of input electrical power deposited into water-cooled anode versus specific energy at various 1:2 nitrogen/hydrogen mixture propellant flow rates. Open symbols represent a facility background pressure nominally 20 Pa, and closed represent a pressure nominally 0.20 Pa.

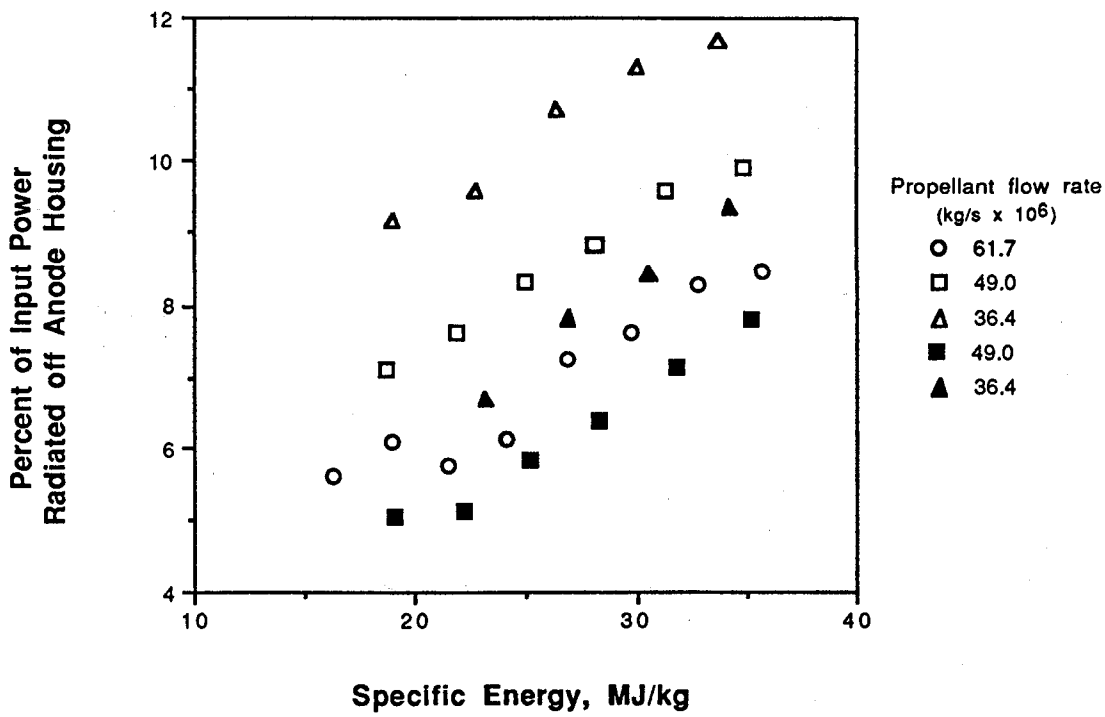

Figure 18. Fraction of input electrical power radiated off anode housing versus specific energy at various 1:2 nitrogen/hydrogen mixture propellant flow rates. Open symbols represent a facility background pressure nominally 20 Pa, and closed represent a pressure nominally 0.2 Pa.

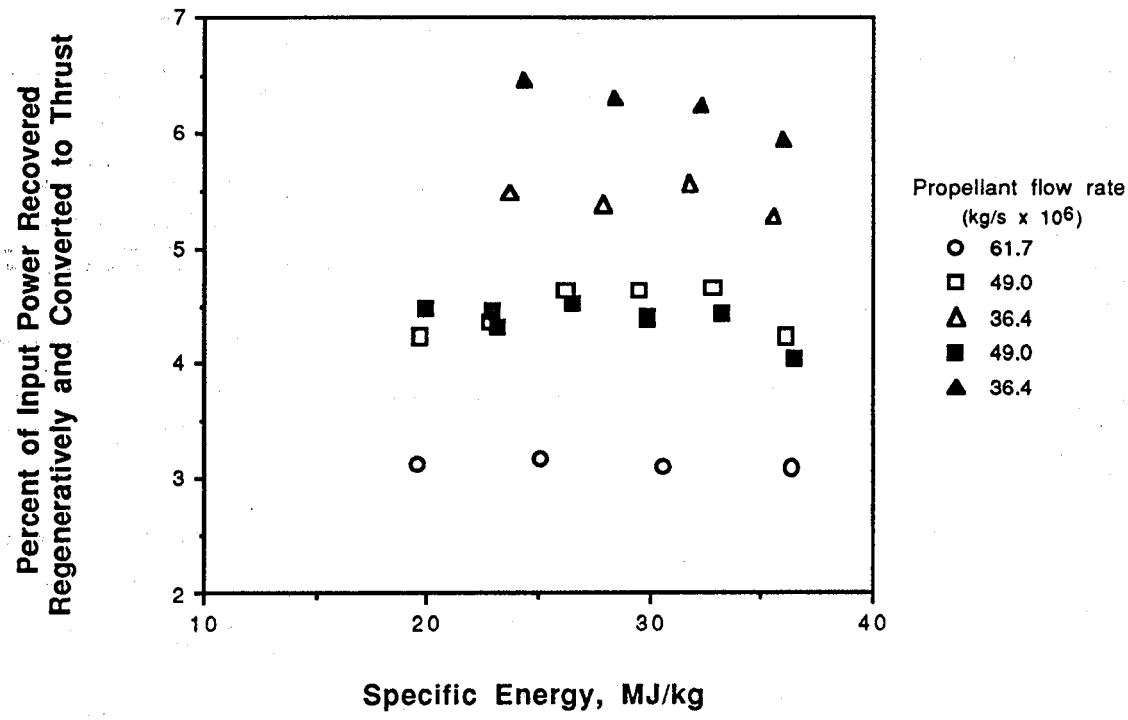

Figure 19. Fraction of input power recovered regeneratively and converted to thrust versus specific energy for radiation-cooled arcjet operating at various 1:2 nitrogen/hydrogen mixture propellant flow rates. Open symbols represent a facility background pressure nominally 20 Pa, and closed represent a pressure nominally 0.2 Pa.

NASA
National Aeronautics and Space Administration

Report Documentation Page

1. Report No.	2. Government Accession No.	3. Recipient's Catalog No.
NASA TM-105156 AIAA-91-2456		

4. Title and Subtitle	5. Report Date
Arcjet Thermal Characteristics	
	6. Performing Organization Code

7. Author(s)	8. Performing Organization Report No.
John M. Sankovic and Francis M. Curran	E-6442
	10. Work Unit No. 506-42-31

9. Performing Organization Name and Address	11. Contract or Grant No.
National Aeronautics and Space Administration Lewis Research Center Cleveland, Ohio 44135-3191	
	13. Type of Report and Period Covered Technical Memorandum

12. Sponsoring Agency Name and Address	14. Sponsoring Agency Code
National Aeronautics and Space Administration Washington, D.C. 20546-0001	

15. Supplementary Notes

Prepared for the 27th Joint Propulsion Conference cosponsored by the AIAA, SAE, ASME, and ASEE, Sacramento, California, June 24-27, 1991. Responsible person, John M. Sankovic, (216) 433-2409.

16. Abstract

The performance of radiation-cooled and water-cooled arcjet thrusters operating on both 1:2 nitrogen/hydrogen mixtures at 1-2 kW and on pure hydrogen at 1-4 kW were compared. For the radiation-cooled thruster, the thrust power recovered regeneratively was evaluated experimentally, and the anode losses were measured by the use of a radiant heat calorimeter. Anode power deposition was measured calorimetrically for the water-cooled design. The fraction of input electrical power lost to the anode increased with specific energy. In all cases, anode losses at a given specific energy level decreased with an increase in propellant flow rate. The data suggest that increases in flow rate decrease the anode losses by decreasing the anode fall voltage. The fraction of electrical power recovered regeneratively and converted to thrust decreased with increasing flow rate. To investigate the effects of test facility background pressure on performance, data were taken for both thrusters operating on nitrogen/hydrogen mixtures at facility background pressures nominally at 20 Pa and 0.20 Pa. Increasing the background pressure decreased the thruster performance, and simple pressure area corrections alone could not account for the observed degradation in performance. Increased facility pressures caused increased anode losses which may account for the remainder of the performance degradation.

17. Key Words (Suggested by Author(s))	18. Distribution Statement
Arcjet engines; Thermal analysis; Heat transfer; Anodes; Nozzles; Electric propulsion; Auxiliary propulsion	Unclassified - Unlimited Subject Category 20

19. Security Classif. (of the report)	20. Security Classif. (of this page)	21. No. of pages	22. Price*
Unclassified	Unclassified	30	A03

NASA FORM 1626 OCT 86

*For sale by the National Technical Information Service, Springfield, Virginia 22161